



Murdoch
UNIVERSITY

MURDOCH RESEARCH REPOSITORY

This is the author's final version of the work, as accepted for publication following peer review but without the publisher's layout or pagination.

The definitive version is available at

<http://dx.doi.org/10.1007/s00382-014-2160-2>

**Kala, J., Andrys, J., Lyons, T.J., Foster, I.J. and Evans, B.J.
(2015) Sensitivity of WRF to driving data and physics options on
a seasonal time-scale for the southwest of Western Australia.
Climate Dynamics, 44 (3-4). pp. 633-659.**

<http://researchrepository.murdoch.edu.au/22664/>

Copyright: © 2014 Springer-Verlag Berlin Heidelberg.

It is posted here for your personal use. No further distribution is permitted.

Sensitivity of WRF to driving data and physics options on a seasonal time-scale for the southwest of Western Australia

Jatin Kala · Julia Andrys · Tom J. Lyons · Ian J. Foster · Bradley J. Evans

Received: date / Accepted: date

1 **Abstract** Regional climate models are sensitive to the forcing data used, as well as
2 different model physics options. Additionally, the behaviour of physics parameteri-
3 sations may vary depending on the location of the domain due to different climatic
4 regimes. In this study, we carry out a sensitivity analysis of the Weather Research

Jatin Kala

Australian Research Council Centre of Excellence for Climate Systems Science and Climate Change Research Centre, University of New South Wales, Sydney, NSW, 2052, Australia

E-mail: J.Kala@unsw.edu.au

Tom J. Lyons and Julia Andrys

State Centre of Excellence for Climate Change Woodland and Forest Health, Murdoch University, Murdoch, WA, 6150, Australia

Ian J. Foster

Western Australian Department of Agriculture and Food, Bentley, WA, 6102, Australia

Bradley J. Evans

Department of Biological Sciences, Macquarie University, Macquarie Park, NSW, 2113, Australia

5 and Forecasting model to different driving data and model physics options over
6 a 10-km resolution domain in the southwest of Western Australia, a region with
7 Mediterranean climate. Simulations are carried out on a seasonal time-scale, in
8 order to better inform future long-term regional climate simulations for this re-
9 gion. We show that the choice of radiation scheme had a strong influence on both
10 temperature and precipitation; the choice of planetary boundary layer scheme has
11 a particularly large influence on minimum temperatures; and, the choice of cumu-
12 lus scheme or more complex micro-physics did not strongly influence precipitation
13 simulations. More importantly, we show that the same radiation scheme, when
14 used with different driving data, can lead to different results.

15 **Keywords** Dynamical downscaling · Physics parameterisation · Regional climate
16 modeling · WRF

17 1 Introduction

18 The south-west of Western Australia (SWWA, see Fig. 1) is a region of significant
19 agricultural production, with an estimated 13 million hectares of native vegetation
20 cleared for agricultural land-use since the late 1820s (Huang et al, 1995; Andrich
21 and Imberger, 2013). Grains are the main crops grown, with the commodity value
22 of wheat, barley, and oats varying seasonally from approximately \$3,000 million to
23 more than \$5,000 million between 2006 and 2010 (ABS, 2010). The region's crops
24 are grown from winter to spring and rain-fed, and hence, crop yields are impacted
25 heavily by inter-annual variations in temperature and precipitation. SWWA is also
26 home to some of Australia's most iconic forests, which are sensitive to changes
27 in temperature and precipitation (Hughes et al, 1993; Hughes, 2003; Evans and

28 Lyons, 2013). An understanding of the current climate of SWWA and how it might
29 change in the future is therefore crucial for the planning and management of the
30 region's agriculture and forestry sectors.

31 SWWA experiences a Mediterranean climate, with hot and dry summers, and
32 cool and wet winters (Gentili, 1971). Its climate is mainly driven by the position
33 of the subtropical high pressure belt, which brings hot and dry continental air from
34 the interior to the southwest during summer. Continental heating during summer
35 results in surface heat troughs which control the penetration of sea-breezes and
36 modulates temperature along the coast (Ma and Lyons, 2000; Ma et al, 2001).
37 As the subtropical high pressure belt gradually moves northwards during winter
38 and autumn, the region experiences most of its annual rainfall via the passage of
39 frontal systems. Complex interactions between blocking-highs and frontal systems
40 result in cut-off lows which are thought to account for up to 40% of the austral
41 summer and spring rainfall (Pook et al, 2011) in central WA. Summer rainfall
42 is also influenced by the passage of northwest cloud bands (Tapp and Barrell,
43 1984). Coastal regions are influenced by the presence of the Leeuwin Current, an
44 anomalous western boundary current which drives warm tropical waters south-
45 wards (against prevailing winds) resulting in a moderation of winter temperatures
46 and increased rainfall in the region relative to other western coastal margins (Rea-
47 son et al, 1999). The main topographic influence on temperature and precipitation
48 in SWWA is the Darling Scarp (Pitts and Lyons, 1989), which extends 200 km in
49 a north-south direction from approximately 31°S to 34°S roughly 25 km from the
50 coast, representing a sudden increase in topography of about 300 m from sea level
51 (Fig. 1(c)). Previous studies have shown that a minimum horizontal resolution of
52 500 m is required to adequately simulate dynamical features of wind flow along

53 the scarp (Pitts and Lyons, 1990). However, these simulations were restricted to a
54 short time-scale of a few days, and did not explicitly focus on precipitation. Kala
55 et al (2010) carried out longer simulations, focussing on two frontal events but at a
56 lower resolution (20 km), and showed that whilst their model was able to capture
57 the overall precipitation patterns, it was not able to accurately resolve orographi-
58 cally induced precipitation close to the coast due to a poor representation of the
59 scarp.

60 In summary, there is considerable knowledge about the current climate of
61 SWWA, however, there is limited information about current and future impacts
62 at the regional scale. Regional climate models (RCMs) are a widely adopted tool
63 to investigate current and future climatic changes at the regional scale. RCMs
64 can dynamically downscale the synoptic fields from re-analysis products and/or
65 global circulation models (GCMs), usually in the order of 100 to 250 km, to a finer
66 resolution which is relevant at the farm/forest scale (1 to 10 km). An RCM which
67 is being increasingly used for such purposes is the Weather Research and Fore-
68 casting (WRF) Advanced Research (WRF-ARW) modelling system (Skamarock
69 et al, 2008). WRF has been used in regional climate simulations for the continen-
70 tal United States (Liang et al, 2005; Lo et al, 2008; Zhang et al, 2009; Leung and
71 Qian, 2009; Bukovsky and Karoly, 2009; Caldwell et al, 2009; Salathe et al, 2010;
72 Bukovsky and Karoly, 2011), East Asia (Kim and Song, 2010; Yuan et al, 2012), as
73 well as Eastern Australia (Evans and McCabe, 2010), and is one of the RCMs being
74 used for the Coordinated Regional climate Downscaling Experiment (CORDEX)
75 (Giorgi et al, 2009) within the World Climate Research Program. WRF can be
76 operated under a variety of configurations which can lead to varying results (e.g.,
77 Lo et al, 2008; Bukovsky and Karoly, 2009; Argüeso et al, 2011; Awan et al, 2011;

78 Evans et al, 2011), and hence it is crucial to test for the most appropriate model
79 setup for a particular purpose over a given region/domain.

80 Different model versions and various settings of WRF were tested by Bukovsky
81 and Karoly (2009) for the continental United States over a 4-month period. They
82 generally recommend the use of Sea Surface Temperature (SST) updates, no inner
83 nest feedback (i.e., no 2-way nesting), use of the NOAH land surface scheme (Ek
84 et al, 2003) rather than the less complex 5-layer diffusion scheme, and the Kain-
85 Frisch (KF) scheme (Kain, 2004) for convection. The effects of different WRF
86 parameterisations were tested on a yearly time-scale for the European Alpine re-
87 gion (Awan et al, 2011), and it was found that parameterisations were sensitive to
88 not just the region, but also the season. For example, cumulus and microphysics
89 schemes have a stronger influence during summer months, while the PBL and ra-
90 diation schemes have an influence throughout the year. This was related to the
91 land-surface having a stronger influence as compared to large-scale synoptic fields,
92 due to stronger surface heating during summer months. Overall, their best model
93 performance was achieved by using the KF scheme for convection (cumulus pa-
94 rameterisation); the Yonsei University (YSU) scheme (Hong et al, 2006) for the
95 PBL with the Monin-Obukhov (MO) scheme for the surface layer; and the Dud-
96 hia scheme (Dudhia, 1989) for radiation. Awan et al (2011) also reported their
97 results to be region specific, namely, that WRF tends to over-predict precipitation
98 in mountainous regions during both summer and winter months.

99 Argüeso et al (2011) investigated different WRF parameterisations for regional
100 climate simulations over Southern Spain for a 10-year period. They determined
101 that the cumulus and PBL schemes had a crucial impact on precipitation whereas
102 the microphysics scheme had no noticeable impact. Minimum temperatures were

103 sensitive to the choice of PBL scheme. Overall, they found that the combina-
104 tion of the Betts-Miller-Janjic (BMJ) cumulus scheme (Betts, 1986; Betts and
105 Miller, 1986; Janjić, 1994, 2000) with the Asymmetric Convective Model (AC2)
106 PBL scheme (Pleim, 2007a,b) and the WRF single moment 3-class microphysics
107 scheme to perform the best. Flaounas et al (2011) and Crétat et al (2011) in-
108 vestigated the impacts of different convective and PBL schemes over Africa and
109 found that the choice of PBL schemes have the strongest effect on temperature,
110 and that precipitation variability was strongly influenced by the choice of convec-
111 tive parameterisation scheme. Evans et al (2011) carried out a 36-member WRF
112 physics ensemble for storm events on the east coast of Australia. They found that
113 whilst no particular combination of schemes performed best for all events, vari-
114 ables and metrics, the MYJ PBL scheme and BMJ cumulus schemes were robust in
115 performance. They suggest that the YSU PBL scheme, KF scheme for convection,
116 and RRTMG radiation scheme should not be used in combination for Eastern Aus-
117 tralia. Evans et al (2011) also point out that the choice of physics scheme becomes
118 more important as rainfall intensity increases.

119 Other than radiation, cumulus, and PBL schemes, the choice of land surface
120 model (LSM) can strongly influence near surface temperature, moisture and winds.
121 Jin et al (2010) investigated four LSMs in WRF and found that the more complex
122 Community Land Model (CLMv3), generally outperformed the simpler NOAH,
123 RUC (Smirnova et al, 2000), and soil thermal diffusion scheme. They found no
124 close relationship between the choice of LSM and precipitation. Prabha et al (2011)
125 investigated the influence of NOAH and RUC LSMs on low-level jet dynamics and
126 found that the RUC LSM performed better as compared to NOAH at lower eleva-
127 tions, but NOAH performed better at higher elevations. They also found that the

128 NOAH LSM resulted in higher vertical mixing as compared to RUC under sta-
129 ble conditions with low winds and high pressure. They however did not examine
130 influences on precipitation. Mooney et al (2012) on the other hand, have shown
131 that LSM choice not only influences temperature, but precipitation simulations,
132 especially during the summer season over Europe. Namely, they showed that use
133 of the NOAH LSM as compared to the RUC LSM, resulted in lower biases for
134 temperature, but simulations using the RUC LSM generally had lower precipita-
135 tion biases as compared to those using NOAH. Finally, a recent study by Stéfanon
136 et al (2013) showed that use of the simple thermal diffusion scheme in WRF does
137 not allow for the accurate simulation of heat-wave conditions over Europe, and
138 more sophisticated LSMs such as the RUC, which explicitly resolve the treatment
139 of soil processes is required.

140 Based on the current literature, it is clear that WRF is sensitive to the domain
141 (location and boundaries), as well as different model parameterisations. Adequate
142 testing of model configuration is therefore essential before carrying out long-term
143 regional climate simulations. Accordingly, the aim of this paper is to test differ-
144 ent model physics parameterisations and input data on simulated precipitation
145 and temperature maxima and minima for SWWA. This forms the first part of a
146 broader research project which aims at carrying out regional climate impact as-
147 sessments for the agricultural and forestry sectors of SWWA. We note that the
148 choice of model horizontal and vertical resolution can be equally important to
149 the choice of boundary conditions and physics options. However, the resolution
150 issue is not explicitly addressed in this paper, as model resolution for long term
151 climate simulation is inherently limited to computational and storage constraints.
152 This paper focuses on finding the best physics options and input forcing data,

153 given these constraints. The next section describes the numerical experiments car-
154 ried out, followed by a description of the observational data-sets and statistical
155 analysis used.

156 **2 Methods**

157 2.1 Numerical Experiments

158 Yearly simulations were carried out with WRF-ARW Version 3.3 from October
159 2009 to November 2010, with the first two months being model spin-up and not
160 used in the analysis. Two nested grids (1-way nesting) were used spanning 5150 km
161 \times 4200 km and 1760 km \times 1440 km, at 50 km and 10 km resolutions respectively
162 as shown in Figs. 1 (a) and (b). Both nested grids used 30 vertical levels, with
163 levels more densely spaced within the PBL. Given the relatively long simulation
164 period, use of nudging techniques was required to prevent model drift. This is
165 commonly used for regional climate simulations (e.g., Argüeso et al, 2011) to ensure
166 that the simulations retain the large scale features important in regional climate
167 modeling. Based on previous studies which have investigated the influence of grid
168 (analysis) versus spectral nudging techniques (Lo et al, 2008; Bowden et al, 2011;
169 Liu et al, 2012; Omrani et al, 2013), we opted for spectral nudging applied to
170 the outer domain (50 km) and above the PBL. Deep soil temperatures were set
171 to a 150-day lagged averaging period and a series of sensitivity tests were carried
172 out by changing the source of lateral boundary-conditions, SSTs, and the following
173 model parameterisation schemes as outlined in Table 1; LSM, cumulus/convective,
174 longwave and shortwave radiation, PBL, and cloud-microphysics.

175 The reference experiment (REF) was chosen because it follows the same con-
176 figuration as in Evans and McCabe (2010) (except that Evans and McCabe (2010)
177 used WRF3.0.1) which has shown adequate results for southeast Australia. REF
178 uses 6-hourly boundary conditions from the 2.5×2.5 degree resolution National
179 Centre for Atmospheric Research (NCAR) / National Centre for Environmental
180 Prediction (NCEP) (commonly referred to as NNRP); the NOAA land surface
181 model (LSM) (Chen and Dudhia, 2001a,b); the Rapid Radiative Transfer Model
182 (RRTM) (Mlawer et al, 1997) and Dudhia schemes for long wave and shortwave
183 radiation respectively; the KF scheme for convection; the YSU PBL scheme with
184 MO surface layer scheme; surface skin temperatures within the NNRP data as
185 SSTs; and the 5-class single moment microphysics scheme (WSM 5-Class).

186 Experiment N_SST is the same as REF, except that weekly mean SSTs from
187 the National Oceanic and Atmospheric Administration (NOAA) SST product is
188 used (Reynolds et al, 2002) and are interpolated to 6-hourly fields for use in WRF.
189 The NOAA SST is at a 1.0×1.0 degree resolution and derived from satellites and
190 in-situ measurements. On the other hand, NNRP data used in REF incorporate
191 an earlier version of the same SST data-set (Reynolds and Smith, 1994), which
192 are interpolated to daily values and used in the coupled ocean-atmosphere data
193 assimilation system (Kalnay et al, 1996) to produce the NNRP product. When
194 running WRF for the REF simulation, these SST data are not used directly, and
195 the surface skin temperature output from NNRP is used instead, as the source
196 of SST in WRF. Hence, the difference between experiments N_SST and REF is
197 that N_SST uses a higher resolution SST in a direct fashion, whereas REF has
198 a lower resolution, and indirectly incorporates satellite estimates of SST. This is

199 illustrated in Fig. 2 for JJA (winter) and SON (spring) showing that NOAA SSTs
200 are higher by up to 1.4°C close to the coast.

201 Experiments FNL and ERA are the same as REF, except that the 6-hourly
202 boundary conditions are taken from the 1.0×1.0 degree NCEP Final (NCEP-
203 FNL) Operational Global Data Assimilation System and the 1.5×1.5 degree
204 ERA-interim (ERA-Int) re-analysis product (publicly available version) from the
205 European Centre for Medium-Range Weather Forecasts (ECMWF) respectively.
206 The NCEP-FNL data includes observations from the Global Telecommunications
207 Systems and many other data sources, and is generated using the same model used
208 by NCEP for their Global Forecast System (GFS). NCEP-FNL data are prepared
209 after GFS is initialised such that the observational data can be used, but the
210 product is only available from late 1999 to present. The ERA-Int data emanates
211 from the ECMWF's ERA-40 product and involves better representations of the
212 hydrological cycle, quality of the stratospheric circulation, handling of biases, and
213 use of observations. The data are available from 1979 onwards and more detail can
214 be found in Dee et al (2011). These experiments were carried out because, as to
215 the author's knowledge, no previous study has explicitly compared these three re-
216 analysis products in WRF. Additionally, these simulations will help better inform
217 the influence of using data from different sources (e.g., different GCMs) as input
218 forcing for future climate projections for future studies in this region.

219 The RUC simulation differs from REF in that it uses the RUC LSM (Smirnova
220 et al, 2000), rather than the NOAH LSM (Chen and Dudhia, 2001a,b). This ex-
221 periment was carried out as the choice of LSM can have a large influence on tem-
222 perature and precipitation (e.g., Prabha et al, 2011; Mooney et al, 2012; Stéfanon
223 et al, 2013). Whilst the NOAH LSM is the most commonly used LSM in WRF for

224 regional climate modelling (e.g., Evans and McCabe, 2010; Argüeso et al, 2011;
225 Awan et al, 2011; Argüeso et al, 2012), the RUC LSM is of comparable complexity
226 but has not been as extensively evaluated.

227 The BMJ simulation differs from REF in that the BMJ scheme is used for con-
228 vection rather than KF. The choice of convective scheme can have a strong influ-
229 ence on precipitation simulations (Bukovsky and Karoly, 2009; Argüeso et al, 2011;
230 Awan et al, 2011). Whilst the majority of studies use the KF scheme (Bukovsky
231 and Karoly, 2009; Evans and McCabe, 2010; Awan et al, 2011), Argüeso et al
232 (2011) found the BMJ scheme performed better for their simulations. Experiments
233 RRTMG and CAM consider different radiation schemes; RTG uses a modified
234 version of the shortwave RRTM scheme for application in GCMs, RRTMG , for
235 both longwave and shortwave radiation and the Community Atmosphere Model
236 schemes are used for longwave and shortwave radiation in the CAM experiment.
237 The accurate resolution of shortwave and longwave radiation is essential for mod-
238 elling low level temperatures, and the PBL and the radiation schemes tested in
239 this experiment tackle the problem in different ways. The CAM schemes use a
240 Delta-Eddington approximation for shortwave radiation absorption and scatter-
241 ing (Collins et al, 2004), and the RRTMG model, like the RRTM model, uses
242 the correlated-k method for radiative transfer (Iacono et al, 2008). Both CAM
243 and RRTMG schemes use overlapping cloud fraction algorithms to determine the
244 cloudiness of the grid whereas the RRTM/Dudhia parameterisaion considers only
245 a binary measure of grid cloudiness. CAM and RRTMG radiation schemes differ
246 further from Dudhia/RRTM in that they take into account the concentrations
247 of trace gases, aerosols, ozone, and carbon-dioxide, and they consider reflected
248 shortwave radiation fluxes.

249 PBL and land surface schemes are varied in experiments AC2 and AC2_P.
250 These experiments differ from REF through the use of the AC2 scheme for PBL
251 with the MO land surface scheme in the case of experiment AC2 and with the
252 Pleim-Xiu (PX) surface layer scheme (Pleim, 2006) in experiment AC2_P. These
253 experiments were undertaken as a result of Argüeso et al (2011) findings that the
254 AC2 scheme performed better for their simulations as compared to the more widely
255 used YSU/MO schemes. The PX scheme was also tested as the AC2 scheme can
256 be used in conjunction with both the MO and PX schemes.

257 Simulations 3C and 5C_D test the sensitivity of microphysics schemes. The
258 3C experiment is the same as in REF, except it employs the simpler 3-class mi-
259 crophysics, rather than the more complex 5-class scheme used in REF. The 3-
260 class scheme only resolves 3 states of cloud water, namely water/ice, vapour, and
261 rain/snow, whereas the 5-class scheme includes cloud water and ice, rain, snow,
262 and vapour. The 5C_D experiment employs the double moment 5-class scheme
263 rather than the single moment scheme of the REF experiment. The double moment
264 scheme computes hydrometeor number concentrations, allowing for more flexibil-
265 ity, whereas the single moment schemes have a pre-defined distribution function
266 for hydrometeor sizes (Lim and Hong, 2009). As a rule of thumb, high resolution
267 simulations of individual storm events usually require more complex microphysics
268 parameterisations, which may not be necessary for regional climate runs (from a
269 computational perspective) hence it is useful to test several schemes to strike the
270 right balance. We note that more complex 6-class schemes exist in WRF which
271 include graupel, however, this form of precipitation is rarely observed in SWWA,
272 and hence these schemes were not tested.

273 The final two experiments, FNL_RTG and ERA_RTG, were conducted as a
274 consequence of the results from the experiment RTG which will be discussed
275 later. These simulations differ from the REF experiment because they employ
276 the RRTMG radiation scheme (for both longwave and shortwave radiation), and
277 they use the NCEP-FNL (FNL_RTG) and ERA-Int (ERA_RTG) lateral boundary
278 conditions.

279 2.2 Observations, regionalisation and data analysis

280 Daily gridded observations of precipitation and maximum and minimum temper-
281 atures were obtained from the Australian Bureau of Meteorology (BoM) (Jones
282 et al, 2009) as part of the Australian Soil Water Availability Project (AWAP)
283 (Raupach et al, 2008, 2009). These data are at a resolution of $0.05^\circ \times 0.05^\circ$ (ap-
284 proximately $5 \text{ km} \times 5 \text{ km}$) and are obtained by interpolating data from a network
285 of stations (Jones et al, 2009). The number of stations used varies with time and
286 their location are shown as the white dots in Figs. 4a and 4b for precipitation and
287 temperature respectively. The AWAP data-set has been previously used in evalu-
288 ating climate simulations over Australia (Evans and McCabe, 2010; Evans et al,
289 2011). King et al (2013) evaluated the AWAP data-set against station observations
290 for extreme rainfall events and found that whilst the product tends to underes-
291 timate the frequency of heavy rainfall events and overestimate that of very low
292 rainfall events, it generally performs reasonably well in capturing the inter-annual
293 variability of extreme rainfall events, and their spatial extents. The latter caution
294 against the use of AWAP when the aim is to examine trends and variability in
295 extremes in regions with poor coverage of station locations. This is not an issue for

296 this study as the focus is on the ability of WRF to simulate the seasonal variation
297 over a one year period.

298 An initial comparison of the WRF output to the BoM AWAP gridded data
299 showed that the model had errors specific to particular land use regions within
300 the model domain. Considering these particularities, we distinguish 3 regions as
301 illustrated in Fig. 3; the coastal region, agricultural region and the predominantly
302 inland rangelands. The northern reaches of the coastal region accommodates the
303 overwhelming majority of the SWWA population in the Perth metropolitan area
304 and the south and east of the region contains most of the remaining forest in the
305 SWWA. The agricultural region, which consists almost exclusively of cereal crops
306 in the winter and spring and bare earth for the remainder of the year, is physically
307 bounded to the east by nature reserves and a vermin proof fence (Lyons et al,
308 1993), but it is constrained also by the rainfall gradient, which declines markedly
309 from west to east as the distance from the coast increases (Fig. 4(a)). The eastern
310 boundary of the agricultural region is therefore the approximate limit at which
311 rain fed crops are viable. The rangelands region, which comprises the majority of
312 the SWWA is a semi-arid to arid zone which is sparsely vegetated and remains
313 in a relatively pristine state. As defined, these land use regions are particularly
314 relevant for management of the agriculture and forestry sectors in the SWWA
315 however they also represent different climatic regions, particularly with respect to
316 rainfall; with the coastal region receiving the majority of the rainfall while the
317 agricultural region receives on average about half the rainfall of the coast which
318 is a combination of frontal and convective processes. Statistics were computed for
319 each region (Fig. 3) after removing the relaxation zone from the grid boundaries,

320 and shown in Taylor diagrams (Taylor, 2001) and bias plots (biases are shown in
321 absolute and percentage terms, i.e., scaled by the mean of the observations).

322 Whilst the use of a gridded data-set such as AWAP is very useful in evaluating
323 WRF, it has limited use in investigating the intensity, location, and frequency
324 of rainfall events. To this end, we also selected 3 precipitation stations, one in
325 each region, to carry out a time-series analysis. These stations are shown in Fig. 3
326 and were chosen because they are Bureau of Meteorology stations with long term
327 quality controlled data and are on approximately the same latitude.

328 2.3 Climatology

329 The BoM-AWAP data is illustrated in Fig. 4 showing the seasonal mean sum-
330 mer (December-January-February or DJF), autumn (March-April-May or MAM),
331 winter (June-July-August or JJA), and spring (September-October-November or
332 SON) precipitation, maximum temperatures, and minimum temperatures for 2010.
333 During DJF, precipitation is mostly confined inland and brought about by North-
334 West cloud bands and surface convection. Precipitation increases during MAM
335 and JJA as the cold-fronts associated with the sub-tropical high pressure cells
336 move further North, with maximum precipitation during JJA and a distinct East-
337 West gradient. Precipitation decreases on the West coast during SON as the cold-
338 fronts move further South, and North-West cloud bands and convection lead to
339 precipitation further inland. Maximum and minimum temperatures both show a
340 North-South gradient, with the highest temperatures confined to the North-West
341 and coolest temperatures to the South-West.

342 Figure 5 shows the seasonal anomalies for precipitation and maximum and
343 minimum temperatures for 2010 over the period 1970-2010. 2010 was clearly a
344 dryer than average year, especially during JJA (winter) and SON (spring), and
345 warmer than average, especially in SON, DJF (summer), and MAM (autumn)
346 during the day (maximum temperatures), but cooler than average in JJA during
347 the night (minimum temperatures). This overall warming and drying trend has
348 been observed since the mid 1970's from streamflow and station observations and
349 been consistent to date (Bates et al, 2008). The overall warming and drying trend
350 is also consistent with future climate projections for this region. Namely, Moise
351 and Hudson (2008) conducted an analysis of IPCC AR4 coupled ocean-atmosphere
352 GCMs, and found that all of them consistently predict a 25-30% decrease in win-
353 ter rainfall for southwest Australia. The more recent IPCC AR5 report (Collins
354 et al, 2013) also identifies SWWA as a region of strong agreement for decreases in
355 maximum 5-day precipitation and increase in consecutive dry days. Hence, whilst
356 the choice of 2010 does not constitute an average year in a climatological sense,
357 it is representative of future changes in climate for this region. Since the aim of
358 this study is to investigate a WRF configuration which will be used for regional
359 climate projections, the choice of 2010 (drier and warmer than average) is partic-
360 ularly relevant.

361 **3 Results**

362 Before analysing the influence of the different forcing data and physics options, we
363 first briefly examine the effect of the use of the higher resolution 10-km inner nested
364 grid as compared to the outer 50-km grid, as illustrated in Fig. 6 showing seasonal

365 precipitation, maximum and minimum temperatures from the REF experiment for
366 the two domains. The main influence of the inner nest is to better resolve coastal
367 processes, especially for precipitation, with the outer domain clearly unable to
368 capture much of the coastal rainfall as compared to the observations (Fig. 4). This
369 is not unexpected as the topography is better resolved for the inner nest (Fig. 1).
370 The influence of the inner 10-km grid on temperature is less evident as compared
371 to precipitation, but similarly, the differences are mostly at the coast (for example
372 JJA minimum temperatures). Both domains show very similar patterns and biases
373 as compared to the observation (Fig. 4).

374 3.1 Temperature

375 Figures 7 and 8 show Taylor diagrams for maximum and minimum temperatures
376 respectively (the coastal region is represented by squares, the agricultural region
377 by triangles, and the rangelands by circles). The arc on the Taylor diagrams show
378 the spatial correlation pattern, while the horizontal and vertical axes represent
379 the ratio of the variance of the model to the observations. The dashed concentric
380 circles represent the centred pattern root-mean-square (RMS) difference. Hence,
381 for a perfect model, the point should lie on the 1:1 curved line (equal variance
382 to the observations), and as close as possible to the horizontal axis (zero RMS
383 difference and pattern correlation of one). Absolute and percentage biases are
384 shown in Tables 2 and 3.

385 All simulations show high pattern correlation of 0.8 to 1.0 for maximum tem-
386 peratures. The RMS errors and relative variances are higher during JJA (austral
387 winter) as compared to the other seasons. Maximum temperatures are simulated

388 well by the REF experiment in terms of correlation, RMS error, and variance how-
389 ever there is a systematic negative bias which is highest in DJF and SON, between
390 3-4 °C. There is considerable variation in the bias between the regions however,
391 there is no consistency between the seasons in this regard; for example, the coastal
392 region is simulated with the least bias in MAM but in SON the coastal bias exceeds
393 that of both the agricultural region and rangelands. This may be partly due to
394 the fact that the regionalisation used reflects the east-west precipitation gradient,
395 whereas the temperature gradient is, as expected, north-south. This is clearly a
396 shortfall of this study, and a separate regionalisation for temperature could be
397 more appropriate. However, the context here is to provide future climate informa-
398 tion to the agricultural and forestry sectors, and hence, we use a regionalisation
399 based on broad land-use classes.

400 Reflecting the trend observed in maximum temperatures, night time minimum
401 temperatures are also systematically underestimated by the REF experiment how-
402 ever there is considerably less variation in the bias between the coastal, rangeland
403 and agricultural regions. The percentage bias is also greater for minimum tem-
404 peratures than for maximum; biases were generally below 12% of maximum tem-
405 peratures however minimum temperature biases are generally greater than 12%,
406 and in some cases (the winter minima in the agricultural region and rangelands)
407 bias exceeds 50%. The correlation of both minimum and maximum temperatures
408 in the REF experiment were high, except for some simulations during JJA for the
409 rangelands (low density of station observations) and the variance ratio was less
410 than 2, showing good performance.

411 The N_SST experiment results were very similar to that of the REF experiment
412 showing that use of NOAA SSTs rather than skin temperatures within NNRP has

413 little influence on temperatures. The FNL and ERA simulations however, demon-
414 strate significantly lower bias relative to the REF experiment, and all experiments
415 driven by NNRP boundary conditions, for maximum temperatures, especially in
416 the warmer months (DJF, MAM and SON). Both simulations had a slight positive
417 bias for minimum temperatures. While the correlations of these experiments are
418 high, they do exhibit some noticeable differences in variance between models and
419 observations when compared to the NNRP driven experiments, particularly with
420 respect to minimum temperatures. For example, when compared to REF, RMS
421 errors and the variance ratio are higher during DJF at the coast and in the agricul-
422 tural regions. However, for impact studies focussing on agriculture and forestry, it
423 is temperature extremes, rather than variability, which has the strongest impact.
424 Hence, the reduction in bias is a major advantage of using the FNL and ERA-
425 interim data-sets over the NNRP. We also note that while both sets of driving
426 data perform better than NNRP, there is however little difference between the
427 performance of these two re-analysis packages. Of particular relevance to agricul-
428 ture is surface soil moisture and temperature and an examination of the differences
429 between the 3 re-analysis showed that FNL and ERA had higher surface soil tem-
430 peratures as compared to REF by 2-3 °C (not shown), reflecting the lower screen
431 temperature bias for these two experiments as compared to REF (Tables 2 and 3).
432 The FNL and ERA experiments also showed slightly higher soil moisture as com-
433 pared to REF by about 0.05-0.1 m⁻³ m⁻³ which can be explained by the higher
434 precipitation for these two experiments, discussed later in section 3.2.

435 The RUC experiment has large positive biases as compared to the REF ex-
436 periment for maximum temperature ranging from 5 to 9°C especially during the
437 SON, DJF, and MAM seasons (Table 2), whilst the biases for minimum temper-

438 ature were slightly lower as compared to REF (Table 3). The Taylor diagram for
439 maximum temperature (Fig. 7) shows that the RUC experiment had large variance
440 ratios as well as RMS error, especially for JJA and SON, as compared to REF ex-
441 periment, whilst there were no marked differences for minimum temperature (Fig.
442 8). Figure 9 shows the seasonal differences in sensible and latent heat flux between
443 the REF and RUC experiments. During DJF and SON, the RUC experiment had
444 higher sensible heat over most of the agricultural region and rangelands by about
445 $15\text{-}30\text{ W m}^{-2}$ and lower latent heat flux by about $5\text{-}15\text{ W m}^{-2}$, reflecting the
446 large biases in maximum temperature. Differences in soil moisture between the
447 two experiments were less than $0.1\text{ m}^{-3}\text{ m}^{-3}$.

448 The BMJ experiment results were very similar to the REF experiment, show-
449 ing little change in bias or RMS and variance ratio or spatial correlation pattern.
450 Changing the radiation scheme showed more interesting results. CAM shows a
451 slight reduction in negative bias relative to the REF experiment however the im-
452 provement observed by the use of the RRTMG radiative scheme for longwave and
453 shortwave radiation (in experiment RTG) is significant, and produces the strongest
454 model performance across all simulations driven by NNRP boundary conditions.
455 In MAM and JJA, the negative bias is almost eliminated entirely by the RTG
456 experiment and there is at least a 1°C improvement in DJF and SON. It was as
457 a result of these findings that the FNL_RTG and ERA_RTG model simulations
458 were run to further assess the merits of the RRTMG scheme when used with the
459 FNL and ERA-interim re-analyses.

460 When the FNL and ERA-Interim boundary conditions are used along with the
461 RRTMG longwave and shortwave radiation schemes in experiments FNL_RTG
462 and ERA_RTG, the results show a reduction in the negative bias for maximum

463 temperatures, indicating some improvement as compared to to the FNL and ERA
464 simulations (Table 2). For minimum temperatures, the FNL and ERA simulation
465 had small positive biases, and use the RRTMG scheme results in an increase
466 in these biases (Table 3), i.e., the net effect of the RRTMG scheme is warmer
467 temperatures. For the REF experiment, the biases were mostly negative both
468 maximum and minimum temperatures, and hence, the RTG simulation showed a
469 reduction in bias for both maximum and minimum temperatures. For the FNL and
470 ERA experiments, biases were negative for maximum temperature, but positive for
471 minimum temperatures, and hence use of the RRTMG scheme in FNL_RTG and
472 ERA_RTG improved the maximum temperature bias, but increased the minimum
473 temperature bias. The net warming effect of the RRTMG scheme (in experiments
474 RTG, FNL_RTG and ERA_RTG) can be explained by the high incoming shortwave
475 radiation as compared to use of the Dudhia scheme (in experiments REF, FNL,
476 and ERA) as illustrated in Fig. 10 showing differences between 15-30 W m^{-2}
477 across the domain for all seasons.

478 Whilst the use of different micro-physics had little to no influence on temper-
479 ature, the use of the AC2 PBL scheme increased the negative bias for maximum
480 temperatures, most notably in DJF, MAM, and SON, especially in the range-
481 lands region. This negative bias is further enhanced when the AC2 PBL scheme
482 is employed in combination with the Pliem Xu surface layer scheme (experiment
483 AC2_P). However, for maximum temperatures, the AC2_P simulations result in
484 lower biases as compared to the AC2 experiment, during DJF and SON. The high
485 negative bias for minimum temperatures can be related to a rapid collapse of
486 the nocturnal PBL as illustrated in Fig. 11, showing the seasonal daily average
487 minimum PBL height for the AC2, AC2_P and REF experiments.

488 3.2 Precipitation

489 Figure 12 shows Taylor diagrams for precipitation and the absolute and percentage
490 biases are shown in Table 4. A clear seasonal pattern is evident for all simulations
491 and regions, with biases, RMS errors and ratio of variances being generally higher
492 during DJF and MAM (austral summer and autumn) and lower during JJA and
493 SON (winter and spring). The weak performance in precipitation for all simulations
494 during summer can be attributed to the difficulty in accurately simulating the
495 intensity of the convective rainfall events which dominate rainfall in summer and
496 autumn, especially in the rangelands region. Winter rain is mostly from frontal
497 systems, i.e., synoptically driven and strongly influenced by the forcing data, and
498 hence, JJA and SON precipitation show lower errors.

499 Biases for the REF experiment are negative except for coastal region during
500 DJF (low rainfall season), showing the WRF generally under-predicts precipita-
501 tion, and additionally, the bias is most negative for the rangelands regions, ranging
502 from -80 to -100 % (a bias of -100% indicates that the model hardly captured any of
503 the observed rainfall). Precipitation in this region is relatively small in magnitude
504 compared to the coast (see Figure 4) and strongly influenced by surface convection
505 all year-round, rather than synoptically driven. Given the spatial paucity of the
506 observational network in the rangelands there is an inherent disconnect between
507 the observation of small scale convective storms and the model's ability to simulate
508 such events.

509 The spatial correlations varied generally between 0.8 and 1.0, showing that
510 WRF reproduced spatial patterns of precipitation reasonably well. Frontal rain-
511 fall, which is the source of most of the precipitation along the coast and in the

512 agricultural region in JJA (Fig. 12c) and SON (Fig. 12d), is well simulated how-
513 ever the negative bias in the REF simulation is not insignificant, particularly in
514 the agricultural areas (55%). Previous studies in the SWWA have highlighted the
515 meteorological importance of the Darling scarp (a sloping, 300m high escarpment,
516 25km inland which runs parallel to the north-south coastline) and the need to run
517 simulations at a very fine scale to capture the influence on precipitation of this
518 topographical feature (Pitts and Lyons, 1990; Kala et al, 2010). Hence, it is likely
519 that the resolution of this simulation is not accounting for the influence of the
520 scarp on frontal rainfall.

521 To better quantify the ability of WRF to simulate the intensity, timing, and
522 frequency of rainfall events, we carried out a station-level comparison of the REF
523 simulated precipitation against 3 stations (Fig. 3), one located in each region
524 and at roughly the same latitude, illustrated in Fig. 13. Close to the coast, the
525 timing of rainfall events is very well captured, with the exception of a large rainfall
526 event in late March, and WRF generally under-predicts precipitation. Within the
527 agricultural and rangelands region, as the intensity of rainfall decreases further
528 from the coast, the REF experiment clearly is unable to capture small rainfall
529 events, especially at the Norseman station. Namely, REF only simulated 3 rainfall
530 events, whereas the observations show well in excess of 15 rainfall events.

531 The use of the NOAA SSTs in the N_SST experiment as compared to the REF
532 experiment results in a reduction in bias for precipitation along the coast and to
533 a lesser degree in the agricultural region during JJA and SON. There is a large
534 increase in percentage bias at the coast and the agricultural region during DJF,
535 however, this corresponds to a very small change in absolute bias. This is expected
536 as DJF rainfall in these regions is relatively small. Figure 2 shows the difference

537 in SST between the N_SST and REF experiments during JJA and SON, and
538 illustrates that the use of surface skin temperature data in the REF experiment
539 as a surrogate for SST is predominantly underestimating SST, especially close
540 to the coast. In terms of winter precipitation, there is merit in employing the
541 satellite derived NOAA SST data as used in the N_SST experiment, especially
542 when simulation domains contain a significant percentage of sea surface, as is the
543 case here. While the NOAA SSTs are providing a benefit in winter coastal model
544 performance, it is however worth noting that, in addition to a slight bias increase
545 in DJF, the N_SST simulation did result in an increase in relative variance and
546 RMS errors for precipitation in the warmer months of DJF and MAM. For this
547 region, accurate simulations of precipitation along the coast during JJA is of prime
548 importance as it is the main source of water for rain-fed agriculture. Hence, we
549 argue that the use of NOAA SSTs is a better option.

550 The FNL and ERA simulations show a clear improvement in bias during MAM,
551 JJA, and SON, as compared to the REF experiment. This is especially noticeable
552 for the rangelands region, with smaller biases during JJA and SON as compared
553 to much larger and negative (close to -100%) bias for the REF experiment. During
554 DJF, the FNL simulation produces a larger bias for the coastal and agricultural
555 regions, as compared to the REF experiment, while the ERA simulation only
556 improves the bias at the coast. However both the ERA and FNL simulations
557 shows higher spatial correlation pattern and lower variance ratio and RMS errors
558 as compared to the REF experiment, but the ERA simulations performs best
559 overall. An examination of the differences in SST between the REF and ERA and
560 REF and FNL simulations did not reveal any clear spatial patterns which could
561 explain the differences in precipitation simulations.

562 Use of the RUC LSM had little influence on precipitation as compared to REF,
563 except for higher RMS error and variance ratio at the coast for MAM and larger
564 negative bias at the coast during JJA. It was interesting to note that although
565 RUC produced less precipitation than REF, as shown by the larger negative bias,
566 the RUC simulations had larger latent heat flux during JJA at the coast, a counter-
567 intuitive result. This suggests that the RUC LSM has a larger evaporative flux as
568 compared to the NOAH LSM when soil water is available (i.e., during MAM and
569 JJA), which could be due to the different treatment of above ground processes (e.g.,
570 vegetation evaporation), surface processes (e.g., run-off), as well as sub-surface
571 processes (root zone drainage) between the two LSMs. To adequately quantify
572 these differences would required running both LSMs offline with the same forcing,
573 which is outside of the scope of this paper.

574 The BMJ simulation had fairly similar biases compared to the REF (which
575 uses the KF scheme) experiment during DJF but smaller ratio of variance and
576 RMS errors, showing a better simulation of variability of precipitation. During
577 MAM, JJA, and SON, the BMJ simulation had higher (more negative) bias at
578 the coast as compared to the REF experiment, but lower variance ratio. Hence,
579 both the KF and BMJ schemes have their merits and disadvantages. However the
580 higher bias during JJA and SON at the coast is not insignificant (almost double)
581 and as such, it appears that the KF scheme may be more appropriate in this case.
582 The RTG and CAM simulations had similar biases to REF, except that the bias
583 at the coast during SON was almost twice as large. SON is the austral spring,
584 and represents a transition from frontal (synoptically driven) precipitation, to the
585 summer regime when surface convection has a larger role. Hence, it appears that
586 the radiation schemes are particularly sensitive during that transition period.

587 The AC2 and AC2_P simulations produced similar results during DJF and
588 MAM, but both simulations had lower bias during JJA at the coast as compared
589 to REF, and the AC2_P simulation showed a slight improvement in bias during
590 SON at the coast. There were no major differences in the variance ratios, RMS
591 errors, and spatial correlations. Similarly, the 3C and 5C_D simulations produced
592 very similar results to the REF experiment for precipitation, i.e., the use of a
593 simpler and less computationally expensive microphysics scheme (3C) appears to
594 be appropriate.

595 The FNL_RTG and ERA_RTG schemes were conducted as result of an im-
596 provement in bias in maximum and minimum temperature when comparing the
597 RTG to the REF simulation discussed earlier in section 3.1. The FNL_RTG and
598 ERA_RTG produced very similar results for precipitation during JJA and SON as
599 compared to the FNL and ERA simulations respectively, but there was a marked
600 increase in bias at the rangelands during DJF and MAM. Namely, the precipitation
601 bias increased from 9.5 and 5.8 mm month⁻¹ during DJF and MAM at the range-
602 lands for the FNL experiment, to 22.3 and 19.0 mm month⁻¹ for the FNL_RTG
603 experiment, and from 8.9 and 9.6 mm month⁻¹ to 21.3 and 25.3 mm month⁻¹
604 for the ERA as compared to the ERA_RTG experiment (Table 4). However, no
605 such increase in bias was observed for the RTG experiment as compared to the
606 REF experiment, showing that the RRTMG scheme results in different behaviour
607 with different sources of driving data. We further explored this by examining the
608 changes in convective available potential energy (CAPE), lifting condensation level
609 (LCL), and precipitable water (PW) between the REF, FNL, and ERA simula-
610 tions (i.e., using the Dudhia/RRTM shortwave/longwave schemes) and the RTG,
611 FNL_RTG, and ERA_RTG (i.e., using the RRTMG/RRTMG shortwave/longwave

612 scheme), as illustrated in Fig. 14. Use of the RRTMG scheme clearly results in an
613 increase in CAPE between 60-140 J kg⁻¹ during DJF and MAM for the FNL_RTG
614 and ERA_RTG simulations as compared to FNL and ERA respectively, whilst the
615 differences in CAPE between RTG as compared to REF is much smaller. Higher
616 CAPE implies larger positive buoyancy and higher likelihood of convection and as-
617 sociated precipitation. Additionally, use of the RRTMG scheme clearly resulted in
618 lower LCL and higher PW for all seasons within the rangelands for the FNL_RTG
619 and ERA_RTG simulations as compared to FNL and ERA respectively. Hence,
620 the increased positive buoyancy, lower LCL and larger amount of PW can explain
621 the large positive precipitation biases.

622 **4 Discussion**

623 The REF experiment provided a reasonable simulation at the seasonal scale for
624 the domain of the interest. However, the negative biases for maximum and min-
625 imum temperatures are not insignificant, given that impacts on agriculture and
626 forestry are not only dependant on precipitation, but also temperature extremes
627 (van Gool and Vernon, 2005; Lobell et al, 2012). Additionally, given the known
628 issues of low moisture availability within the NNPR data-set for the southern hemi-
629 sphere (Schneider et al, 2013), this combined with negative temperature biases,
630 may partly explain the overall negative bias in precipitation as well. The temper-
631 ature biases were reduced when using the FNL and ERA-interim re-analyses as
632 forcing data. The better performance when using the ERA-interim and FNL re-
633 analysis as compared to the NNRP is not unexpected, as the former have higher
634 resolution, use more observational data and involve more accurate representations

635 of the hydrological cycle (Dee et al, 2011). The better performance of ERA-Interim
636 over NNRP has also been shown by Fersch et al (2012), who compared terres-
637 trial water storage from WRF simulations over Australia (amongst other regions)
638 with both re-analysis against remotely sensed estimates and showed that ERA-
639 Interim driven simulations had lower biases as compared to NNRP, which had a
640 dry tendency. This is in-line with our results which showed large negative biases in
641 precipitation during winter for REF, but smaller positive biases for the ERA sim-
642 ulation. However, it must be noted that the resolution of NNRP is closer to that
643 of GCMs and using NNRP may be more appropriate to enable comparisons with
644 GCM forced simulations. However, if the focus is to re-produce the past climate
645 as accurately as possible, then the use of ERA-Interim and FNL is more appro-
646 priate. The N_SST simulation, which used satellite derived SSTs with the NNRP
647 re-analysis improved the bias for winter precipitation, showing that care should be
648 taken in using the best available source of SST. This is in line with other studies
649 which have shown that the accurate prescription of SSTs in WRF is critical to
650 simulating extreme precipitation events over eastern Australia (Evans and Boyer-
651 Souchet, 2012). An important source of uncertainty for future climate projections
652 are biases within GCMs used to drive RCMs. Whilst this study did not use any
653 GCM data, the results presented also suggest that any future climate study has to
654 use data from more than one GCM, and additionally, critically examine inherent
655 uncertainties and biases within the driving data used.

656 Use of the RUC land surface model resulted in large positive biases for maxi-
657 mum temperature, especially during the warmer seasons of SON (spring) and DJF
658 (summer). Similar results have been found by Mooney et al (2012) over Europe,
659 with the RUC LSM having a bias for the mean summer air temperature of up

660 to 5 °C whilst the NOAH LSM showed much lower biases (with all other physics
661 options being the same). The biases reported here are higher, ranging from 6 to
662 10 °C (Table 2), since we explicitly focussed on maximum and minimum tem-
663 peratures, while Mooney et al (2012) evaluated the mean temperature. Mooney
664 et al (2012) also reported that the NOAH LSM has a greater tendency to show
665 a positive bias in daily precipitation as compared to the RUC. Here we also find
666 that the NOAH LSM generally results in higher precipitation as compared to RUC
667 with the NOAH LSM having a smaller negative bias as compared to RUC (Table
668 4). Comparison of the surface turbulent heat fluxes showed that the RUC LSM
669 has higher sensible heat flux as compared to the NOAH LSM for DJF and SON,
670 which can explain the temperature bias. However surface heat fluxes are integra-
671 tive of processes with the PBL, and identifying the reasons behind the differences
672 in surface fluxes between the RUC and NOAH LSMs would require running both
673 models offline with the same forcing, which is beyond the scope of this paper.

674 Because of the predominance of convective rainfall, especially during summer
675 months and the results of previous studies (Flaounas et al, 2011; Cr  tat et al, 2011),
676 it was expected that simulated rainfall would be sensitive to different convective
677 and PBL parameterisation schemes. However, we did not find large differences in
678 simulated precipitation when switching from the KF to the BMJ cumulus schemes
679 and from the YSU/MO to the AC2 and AC2_P PBL/Surface layer schemes. This
680 may be due to several reasons. Firstly, we simulated a single year, which was par-
681 ticularly dry. However, whilst our results may be sensitive to the choice of year,
682 the persistent warming and drying trend for this region, from both observations
683 (Bates et al, 2008) and GCM projections (Moise and Hudson, 2008; Collins et al,
684 2013), gives us confidence that the choice of cumulus and PBL schemes have little

685 influence on precipitation for SWWA. Secondly, the amount of convective rainfall
686 during DJF in SWWA, is relatively small, compared to JJA (winter) precipitation,
687 and this may also explain the lack of sensitivity to the different schemes, as pre-
688 vious studies have shown that the influence of different physics options is largest
689 for more extreme precipitation events (Evans et al, 2011), and when focussing
690 explicitly on mesoscale convective events (e.g., Jankov et al, 2005). Conversely,
691 the lack of rainfall sensitivity to microphysics scheme was in line with previous
692 research (Argüeso et al, 2011) and it appears that the simple 3-class single moment
693 micro-physics scheme is sufficient, at least for this region and for such resolution.
694 The most important shortfall remains the accurate simulation of DJF (summer)
695 precipitation, which is not unexpected based on studies for similar meteorological
696 conditions in other regions (Pohl et al, 2011)

697 Of particular note for the precipitation results is the fact that all the simu-
698 lations demonstrate a consistent pattern in the predictive performance of WRF
699 based on the regional groupings; the coastal region is simulated with the greatest
700 skill and the rangelands with the least skill. The potential mechanisms for this
701 pattern include a model response to the rainfall gradient, differences in the type
702 of rainfall, change in land use type or a reduction in the distribution of rainfall
703 monitoring stations. Based on the consistently high density of observations in both
704 the coastal and agricultural regions (Fig 4a), it seems unlikely that observation
705 error is solely responsible for this trend. However, because of the low density of
706 observations in the rangelands, it is probable that the error in this region has been
707 exacerbated by some observational errors, which we are unable to quantify.

708 The sensitivity of WRF to different radiation schemes yielded interesting re-
709 sults. Namely, whilst the model was not very sensitive to the use of the CAM

radiation scheme, it was shown to be sensitive to the RRTMG scheme. RRTMG increased the minimum and maximum temperatures relative to simulations using the RRTM/Dudhia scheme due to higher incoming shortwave radiation for all seasons. This improved the bias with NNRP driven simulation, as the latter had negative biases for both maximum and minimum temperatures. However, use of the RRTMG scheme degraded performance for minimum temperatures when used with NCEP-FNL or ERA-interim, as the increase in incoming shortwave radiation acted to make the small positive biases even larger. The higher incoming shortwave radiation could be explained by the fact that the RRTMG scheme allows for fractions to be applied to sub grid cloud cover, unlike the Dudhia scheme where a grid is either completely cloudy or clear. Similar results have been reported elsewhere. Namely, Evans et al (2011) conducted a WRF physics ensemble over eastern Australia (they use ERA-Interim) and also found that the RRTMG/RRTMG shortwave/longwave scheme generally overestimated temperatures. The RRTMG scheme also resulted in large bias in precipitation in the rangelands during the warmer seasons of DJF and MAM when used with NCEP-FNL and ERA-interim forcing, whereas this was not observed when using NNRP. This was due to the RRTMG scheme resulting in much larger CAPE when used with NCEP-FNL and ERA-Interim data as compared to NNRP. This in conjunction with lower LCL and higher precipitable water, would have led to increased precipitation. Evans et al (2011) also found that the RRTMG radiation, KF cumulus, and YSU PBL physics combination performed consistently poorly for all their simulations of storm events in Eastern Australia. Moreover, sensitivity studies over other regions (Yuan et al, 2012; Pohl et al, 2011; Awan et al, 2011), have found that shortwave radiation

734 schemes in particular, have a strong precipitation response. Hence our results are
735 consistent with previous studies.

736 Changing PBL schemes had a strong influence on temperatures. Namely, use of
737 the AC2 PBL scheme, especially in conjunction with the PX surface layer scheme
738 is clearly not recommended for our domain, due to large biases in minimum tem-
739 peratures in the rangelands region. While both YSU and AC2 utilise non local
740 closure schemes, AC2 reverts to a local closure scheme under conditions of neu-
741 trality or stability, especially at night (Hu et al, 2010). As a consequence of this
742 switch to a local closure scheme, the AC2 PBL scheme has a tendency to suffer
743 from a lack of mixing in the night-time boundary layer, which results in a too rapid
744 collapse, low minimum PBL and hence negative bias with respect to night-time
745 minimum temperatures. Hence, this mechanism can explain the high biases.

746 Whilst the choice of PBL schemes has been shown to influence precipitation
747 simulations in other studies (e.g., Argüeso et al, 2011), this was not the case
748 here. Studies in the SWWA have demonstrated that land cover change can impact
749 boundary layer development and therefore precipitation in the region (Lyons, 2002;
750 Kala et al, 2010; Nair et al, 2011). While each region does demonstrate markedly
751 different land uses, and in the case of the agricultural region extensive land cover
752 change, for these land uses to be influencing precipitation, it was expected that
753 this would be demonstrated through a sensitivity to PBL and surface layer scheme,
754 which was not observed. That the choice of PBL scheme does not appear to in-
755 fluence rainfall sensitivity suggests that the errors in rainfall simulation and the
756 regional differences in model performance are not strongly associated with land
757 use type.

758 **5 Conclusions**

759 We carried out a range of sensitivity experiments with WRF, using different forcing
760 data and model physics options. The aim of this was to better inform the planning
761 of future long-term regional climate simulations for this region with significant
762 agricultural and forestry sectors. Overall, it is clear the control (REF) simulation
763 experimental set-up is adequate for longer term climatic simulations for this region,
764 at least at the seasonal time-scale and 10-km spatial resolution. An important
765 issue remains the systematic underestimation of precipitation at the coast, which
766 could be due to un-resolved topography, and hence future studies should aim
767 at further quantifying the role of the Darling scarp on orographically induced
768 precipitation in SWWA. The lack of precipitation during summer further from the
769 coast suggests land-atmosphere feedbacks are not being adequately captured, and
770 this also requires further investigation. The simulations with different re-analysis
771 products show that when the goal is to establish a base-line climatology, the ERA-
772 interim data-set should be preferred over the FNL and NNRP. When NNRP is
773 nonetheless used, the use of NOAA SSTs should be preferred over the use of surface
774 skin temperatures within the NNRP data-set.

775 Our results show that the choice of PBL scheme can have a large influence on
776 temperatures, and choice of radiation scheme on both temperatures and precipi-
777 tation in SWWA. Consistent with previous studies, we found that the RRTMG,
778 in combination with the YSU PBL scheme, and KF cumulus scheme is not recom-
779 mended. Additionally, the AC2 PBL scheme results in large biases for minimum
780 temperature, and should not be used, at least for the domain of interest here. The
781 KF and BMJ cumulus scheme did not result in significant differences for our do-

782 main, and consistent with several studies, using more complex micro-physics does
783 not improve precipitation simulations. More interestingly, we show that schemes
784 may behave differently with different forcing data-sets, as was shown with the
785 RRTMG radiation scheme. Hence, sensitivity testing should ideally include both
786 use of different physics options as well as forcing data.

787 Future studies will evaluate WRF driven by the ERA-interim re-analysis on a
788 climatic (30 years) time-scale (similar to the ERA simulation here), and evaluate
789 the model at daily, seasonal, and inter-annual time-scales, and additionally, use
790 station and sounding observations, in addition to the AWAP gridded product.
791 This will in turn be used to help inform the design of GCM forced simulations to
792 provide regional information of possible future climatic changes in SWWA.

793 **Acknowledgements** This research is funded by the Australian Grains Research and Develop-
794 ment Grant (MCV00013). All WRF simulations were supported by iVEC (<http://www.ivec.org/>)
795 through the use of advanced computing resources provided by the Pawsey Super-Computing
796 Centre located at Murdoch University, Perth, Western Australia, through the National Com-
797 putational Merit Allocation Scheme. Jatin Kala is supported by the Australian Research
798 Council Centre of Excellence for Climate System Science (CE110001028). Julia Andrys is
799 supported by an Australian Postgraduate Award and a Grains Industry Research Scholarship.
800 NOAA_OLSST_V2 data were provided by the NOAA/OAR/ESRL PSD, Boulder, Colorado,
801 USA, from their Web site at <http://www.esrl.noaa.gov/psd/>. The NNRP and NCEP-FNL
802 data for this study are from the Research Data Archive (RDA) which is maintained by the
803 Computational and Information Systems Laboratory (CISL) at NCAR. NCAR is sponsored
804 by the National Science Foundation (NSF). The original data are available from the RDA
805 (<http://dss.ucar.edu>) in dataset number ds090.0 and ds083.2 respectively. ERA-interim data
806 were obtained from the ECMWF data server (http://data-portal.ecmwf.int/data/d/interim_daily/).
807 The comments of two anonymous reviews helped to further enhance the quality of this manuscript.
808 All this support is gratefully acknowledged.

References

- 809 **References**
- 810 ABS (2010) Australian Bureau of Statistics (ABS) Year Book: Agriculture, Avail-
811 able online at: <http://www.abs.gov.au>
- 812 Andrich MA, Imberger J (2013) The effect of land clearing on rainfall and fresh
813 water resources in western australia: a multi-functional sustainability analysis.
814 International Journal of Sustainable Development and World Ecology 20:549–
815 563, DOI 10.1080/13504509.2013.850752
- 816 Argüeso D, Hidalgo-Muñoz J, Gámiz-Fortis SR, Esteban-Parra MJ, Dudhia J,
817 Castro-Díez Y (2011) Evaluation of WRF parameterizations for climate stud-
818 ies over southern spain using a multistep regionalization. Journal of Climate
819 24:5633–5651, DOI 10.1175/JCLI-D-11-00073.1
- 820 Argüeso D, Hidalgo-Muñoz JM, Gámiz-Fortis SR, Esteban-Parra MJ, Castro-Díez
821 Y (2012) High-resolution projections of mean and extreme precipitation over
822 spain using the wrf model (2070–2099 versus 1970–1999). Journal of Geophysical
823 Research: Atmospheres 117(D12), DOI 10.1029/2011JD017399
- 824 Awan NK, Truhetz H, Gobiet A (2011) Parameterization-induced error character-
825 istics of MM5 and WRF operated in climate mode over the Alpline region: An
826 ensemble-based analysis. Journal of Climate 24:3107–3123
- 827 Bates B, Hope P, Ryan B, Smith I, Charles S (2008) Key findings from the indian
828 ocean climate initiative and their impact on policy development in australia.
829 Climatic Change 89:339–354, DOI 10.1007/s10584-007-9390-9
- 830 Betts AK (1986) A new convective adjustment scheme. Part I: Observational and
831 theoretical basis. Quarterly Journal of the Royal Meteorological Society 112:677–
832 691

- 833 Betts AK, Miller MJ (1986) A new convective adjustment scheme. Part II: Single
834 column tests using GATE wave, BOMEX, ATEX and arctic air-mass data sets.
835 Quarterly Journal of the Royal Meteorological Society 112:693–709
- 836 Bowden JH, Otte TL, Nolte CG, Otte MJ (2011) Examining interior grid nudg-
837 ing techniques using two-way nesting in the WRF model for regional climate
838 modeling. Journal of Climate 25:2805–2823, DOI 10.1175/JCLI-D-11-00167.1
- 839 Bukovsky MS, Karoly DJ (2009) Precipitation simulations using WRF as a
840 nested regional climate model. Journal of Applied Meteorology and Climatology
841 48:2152–2159, DOI 10.1175/2009JAMC2186.1
- 842 Bukovsky MS, Karoly DJ (2011) A regional modeling study of climate change
843 impacts on warm-season precipitation in the central U.S. Journal of Climate
844 24:1985–2002, DOI 10.1175/2010JCLI3447.1
- 845 Caldwell P, Chin HN, Bader D, Bala G (2009) Evaluation of a WRF dy-
846 namical downscaling simulation over california. Climatic Change 95:499–521,
847 10.1007/s10584-009-9583-5
- 848 Chen F, Dudhia J (2001a) Coupling an advanced land surface–hydrology model
849 with the Penn State–NCAR MM5 modeling system. Part I: Model implementa-
850 tion and sensitivity. Monthly Weather Review 129:569–585, DOI 10.1175/1520-
851 0493(2001)129;0569:CAALSH;2.0.CO;2
- 852 Chen F, Dudhia J (2001b) Coupling an advanced land surface–hydrology model
853 with the Penn State–NCAR MM5 modeling system. Part II: Preliminary
854 model validation. Monthly Weather Review 129:587–604, DOI 10.1175/1520-
855 0493(2001)129;0587:CAALSH;2.0.CO;2
- 856 Collins RK M, Arblaster J, Dufresne JL, Fichet T, Friedlingstein P, Gao X,
857 Gutowski W, Johns T, Krinner G, Shongwe M, Tebaldi C, Weaver A, Wehner M

- 858 (2013) Long-term Climate Change: Projections, Commitments and Irreversibil-
859 ity. In: Climate Change 2013: The Physical Science Basis. Contribution of
860 Working Group I to the Fifth Assessment Report of the Intergovernmental Panel
861 on Climate Change [Stocker, T.F., D. Qin, G.-K. Plattner, M. Tignor, S.K.
862 Allen, J. Boschung, A. Nauels, Y. Xia, V. Bex and P.M. Midgley (eds.)]. Cam-
863 bridge University Press, Cambridge, United Kingdom and New York, NY, USA.
864 http://www.climatechange2013.org/images/report/WG1AR5_Chapter12_FINAL.pdf
- 865 Collins WD, Rash PJ, Boville BA, Hack JJ, McCaa JR, Williamson DL, Kiehl
866 JT, Briegleb B (2004) Description of the NCAR Community Atmosphere Model
867 (CAM 3.0). NCAR Technical Note NCAR/TN-464+STR, 266 pp., NCAR
- 868 Crétat J, Pohl B, Richard Y, Drobinski P (2011) Uncertainties in simulating re-
869 gional climate of Southern Africa: sensitivity to physical parameterizations using
870 WRF. *Climate Dynamics* 38:613–634, DOI 10.1007/s00382-011-1055-8
- 871 Dee DP, Uppala SM, Simmons AJ, Berrisford P, Poli P, Kobayashi S, Andrae U,
872 Balmaseda MA, Balsamo G, Bauer P, Bechtold P, Beljaars ACM, van de Berg L,
873 Bidlot J, Bormann N, Delsol C, Dragani R, Fuentes M, Geer AJ, Haimberger L,
874 Healy SB, Hersbach H, Hólm EV, Isaksen L, Kållberg P, Köhler M, Matricardi
875 M, McNally AP, Monge-Sanz BM, Morcrette JJ, Park BK, Peubey C, de Rosnay
876 P, Tavolato C, Thépaut JN, Vitart F (2011) The ERA-interim reanalysis: con-
877 figuration and performance of the data assimilation system. *Quarterly Journal*
878 *of the Royal Meteorological Society* 137:553–597, DOI 10.1002/qj.828
- 879 Dudhia J (1989) Numerical study of convection observed during the winter mon-
880 soon experiment using a mesoscale two-dimensional model. *Journal of Atmo-*
881 *spheric Science* 46:3077–3107

- 882 Ek MB, Mitchell KE, Lin Y, Rogers E, Grunmann P, Koren V, Gayno G, Tarpley
883 JD (2003) Implementation of Noah land surface model advances in the National
884 Centers for Environmental Prediction operational mesoscale Eta model. *Journal*
885 *of Geophysical Research* 108(D22), DOI 10.1029/2002JD003296
- 886 Evans BJ, Lyons T (2013) Bioclimatic extremes drive forest mortality in southwest,
887 Western Australia. *Climate* 1:28–52, DOI 10.3390/cli1020028
- 888 Evans JP, Boyer-Souchet I (2012) Local sea surface temperatures add to extreme
889 precipitation in northeast Australia during La Niña. *Geophysical Research Let-*
890 *ters* 39(10), DOI 10.1029/2012GL052014
- 891 Evans JP, McCabe MF (2010) Regional climate simulation over Australia's
892 Murray-Darling basin: A multitemporal assessment. *Journal of Geophysical Re-*
893 *search* 115:D14,114, DOI 10.1029/2010JD013816
- 894 Evans JP, Ekström M, Ji F (2011) Evaluating the performance of a WRF physics
895 ensemble over South-East Australia. *Climate Dynamics* 39:1241–1258, DOI
896 10.1007/s00382-011-1244-5
- 897 Fersch B, Kunstmann H, Bárdossy A, Devaraju B, Sneeuw N (2012) Continental-
898 scale basin water storage variation from global and dynamically downscaled
899 atmospheric water budgets in comparison with GRACE-derived observations.
900 *Journal of Hydrometeorology* 13:1589–1603, DOI 10.1175/JHM-D-11-0143.1
- 901 Flaounas E, Bastin S, Janicot S (2011) Regional climate modelling of the 2006
902 west African monsoon: sensitivity to convection and planetary boundary layer
903 parameterisation using WRF. *Climate Dynamics* 36:1083–1105
- 904 Gentili J (1971) *Australian Climate Patterns*. Thomas Nelson (Australia) Limited,
905 285 pp.

- 906 Giorgi F, Jones C, Asrar GR (2009) Addressing climate information needs at the
907 regional level: the CORDEX framework. *WMO Bulletins* 58:175–183
- 908 van Gool D, Vernon L (2005) Potential impacts of climate change on agriculture
909 and land use suitability: Wheat. Government of Western Australia, Department
910 of Agriculture and Food, Resource Management Technial Report 295
- 911 Hong SY, Noh Y, Dudhia J (2006) A new vertical diffusion package with an explicit
912 treatment of entrainment processes. *Monthly Weather Review* 134:2318–2341
- 913 Hu XM, Nielsen-Gammon JW, Zhang F (2010) Evaluation of Three Planetary
914 Boundary Layer Schemes in the WRF Model. *Journal of Applied Meteorology
915 and Climatology* 49:1831–1844, DOI 10.1175/2010JAMC2432.1
- 916 Huang X, Lyons TJ, Smith RCG (1995) Meteorological impact of replacing native
917 perennial vegetation with annual agricultural species. *Hydrological Processes*
918 9:645–654
- 919 Hughes L (2003) Climate change and Australia: trends, projections and impacts.
920 *Austral Ecology* 28:423–443
- 921 Hughes L, Westoby M, Cawsey EM (1993) Climate range sizes of *Eucalyptus*
922 species in relation to future climate change. *Global Ecology and Biogeography*
923 Letters 5:23–29
- 924 Hutchinson MF, Stein JA, Stein JL (2009) Geodata 9 second digital elevation
925 model (dem-9s) version 3. <http://www.ga.gov.au/>
- 926 Iacono MJD, Mlawer JS, Shephard EJ, Clough MW, Collins SA, D W (2008)
927 Radiative forcing by long-lived greenhouse gases: Calculations with the AER
928 radiative transfer models. *Journal of Geophysical Research* 112:D13
- 929 Janjić ZI (1994) The step-mountain Eta coordinate model: Further developments
930 of the convection, viscous sublayer, and turbulence closure schemes. *Monthly*

- 931 Weather Review 122:927–945
- 932 Janjić ZI (2000) Comments on “development and evaluation of a convection scheme
933 for use in climate models”. *Journal of Atmospheric Science* 57:3686–3686
- 934 Jankov I, Gallus WA, Segal M, Shaw B, Koch SE (2005) The impact of different
935 WRF model physical parameterizations and their interactions on warm season
936 MCS rainfall. *Weather and Forecasting* 20:1048–1060, DOI 10.1175/WAF888.1
- 937 Jin J, Miller NL, Schlegel N (2010) Sensitivity study of four land surface
938 schemes in the WRF model. *Advances in Meteorology* 2010:11 pages, DOI
939 10.1155/2010/167436
- 940 Jones DA, Wang W, Fawcett R (2009) High-quality spatial climate data-sets
941 for Australia. *Australian Meteorological and Oceanographic Society Journal*
942 58:233–248
- 943 Kain JS (2004) The Kain–Fritsch convective parameterization: An update. *Journal*
944 *of Applied Meteorology and Climatology* 43:170–181
- 945 Kala J, Lyons TJ, Nair US (2010) Numerical Simulations of the Impacts of Land-
946 Cover Change on Cold Fronts in South-West Western Australia. *Boundary-Layer*
947 *Meteorology* 138:121–138, DOI 10.1007/s10546-010-9547-3
- 948 Kalnay E, Kanamitsu M, Kistler R, Collins W, Deaven D, Gandin L, Iredell M,
949 Saha S, White G, Woollen J, Zhu Y, Chelliah M, Ebisuzaki W, Higgins W,
950 Janowiak J, Mo KC, Ropelewski C, Wang J, Leetmaa A, Reynolds R, Jenne R,
951 Joseph D (1996) The NCEP/NCAR 40-year reanalysis project. *Bulletin of the*
952 *American Meteorological Society* 77:437–471
- 953 Kim EJ, Song SY (2010) Impact of air-sea interaction on East Asian summer mon-
954 soon climate in WRF. *J Geophys Res* 115:D19,118, DOI 10.1029/2009JD013253

- 955 King AD, Alexander LV, Donat MG (2013) The efficacy of using gridded data to
956 examine extreme rainfall characteristics: a case study for australia. *International*
957 *Journal of Climatology* 33:2376–2387, DOI 10.1002/joc.3588
- 958 Leung LR, Qian Y (2009) Atmospheric rivers induced heavy precipitation and
959 flooding in the western U. S. simulated by the WRF regional climate model.
960 *Geophysical Research Letters* 36:L03,820, DOI 10.1029/2008GLO036 445
- 961 Liang XZ, Choi HI, Kunkel KE, Dai Y, Joseph E, Wang JXL, Kumar P (2005)
962 Surface boundary conditions for mesoscale regional climate models. *Earth In-*
963 *teractions* 9(18):1–28
- 964 Lim KSS, Hong SY (2009) Development of an effective double-moment cloud
965 microphysics scheme with prognostic Cloud Condensation Nuclei (CCN) for
966 weather and climate models. *Monthly Weather Review* 138:1587–1612
- 967 Liu P, Tsimpidi AP, Hu Y, Stone B, Russell AG, Nenes A (2012) Differences
968 between downscaling with spectral and grid nudging using WRF. *Atmospheric*
969 *Chemistry and Physics* 12:3601–3610, DOI 10.5194/acp-12-3601-2012
- 970 Lo JCF, Yang ZL, Pielke RA (2008) Assessment of three dynamical climate down-
971 scaling methods using the Weather Research and Forecasting (WRF) model.
972 *Journal of Geophysical Research* 113:D09,112, DOI 10.1029/2007JD009216
- 973 Lobell DB, Sibley A, Ivan Ortiz-Monasterio J (2012) Extreme heat effects on wheat
974 senescence in india. *Nature Climate Change* 2:186–189
- 975 Lyons TJ (2002) Clouds prefer native vegetation. *Meteorology and Atmospheric*
976 *Physics* 80:131–140, DOI 10.1007/s007030200020
- 977 Lyons TJ, Huang X, Schwerdtfeger P, Hacker JM, Foster IJ, Smith RCG (1993)
978 Land–Atmosphere Interaction in a Semiarid Region: The Bunny Fence Exper-
979 iment. *Bulletin of the American Meteorological Society* 74:1327–1334, DOI

- 980 10.1175/1520-0477(1993)074;1327:LIIASR;2.0.CO;2
- 981 Ma Y, Lyons TJ (2000) Numerical simulation of a sea-breeze under dominant
982 synoptic conditions at Perth. *Meteorol Atmos Phys* 73:89–103
- 983 Ma Y, Lyons TJ, Blockley JA (2001) Surface influences on the australian west
984 coast trough. *Meteorol Atmos Phys* 68:207–217
- 985 Mlawer EJ, Taubman SJ, Brown PD, Iacono MJ, Clough SA (1997) Radiative
986 transfer for inhomogeneous atmospheres: RRTM, a validated correlated-k model
987 for the longwave. *Journal of Geophysical Research* 102(D14):16,663–16,682,
988 DOI 10.1029/97JD00237
- 989 Moise AF, Hudson DA (2008) Probabilistic predictions of climate change for Aus-
990 tralia and southern Africa using the reliability ensemble average of IPCC CMIP3
991 model simulations. *Journal of Geophysical Research: Atmospheres* 113(D15),
992 DOI 10.1029/2007JD009250
- 993 Mooney PA, Mulligan FJ, Fealy R (2012) Evaluation of the sensitivity of the
994 weather research and forecasting model to parameterization schemes for regional
995 climates of Europe over the period 1990–95. *Journal of Climate* 26:1002–1017,
996 DOI 10.1175/JCLI-D-11-00676.1
- 997 Nair US, Wu Y, Kala J, Lyons TJ, Pielke Sr RA, Hacker JM (2011) The role of
998 land use change on the development and evolution of the west coast trough, con-
999 vective clouds, and precipitation in southwest Australia. *Journal of Geophysical*
1000 *Research* 116(D7):D07,103, DOI 10.1029/2010JD014950
- 1001 Omrani H, Drobinski P, Dubos T (2013) Optimal nudging strategies in re-
1002 gional climate modelling: investigation in a big-brother experiment over the
1003 European and Mediterranean regions. *Climate Dynamics* 41:2451–2470, DOI
1004 10.1007/s00382-012-1615-6

- 1005 Pitts RO, Lyons TJ (1989) Airflow over a two-dimensional escarpment. I: Ob-
1006 servations. *Quarterly Journal of the Royal Meteorological Society* 115:965–981,
1007 DOI 10.1002/qj.49711548810
- 1008 Pitts RO, Lyons TJ (1990) Airflow over a two-dimensional escarpment. II: Hydro-
1009 static flow. *Quarterly Journal of the Royal Meteorological Society* 116(492):363–
1010 378, DOI 10.1002/qj.49711649207
- 1011 Pleim JE (2006) A simple, efficient solution of flux–profile relationships in the
1012 atmospheric surface layer. *Journal of Applied Meteorology and Climatology*
1013 45:341–347
- 1014 Pleim JE (2007a) A combined local and nonlocal closure model for the atmospheric
1015 boundary layer. Part I: Model description and testing. *Journal of Applied Me-*
1016 *teorology and Climatology* 46:1383–1395
- 1017 Pleim JE (2007b) A combined local and nonlocal closure model for the atmospheric
1018 boundary layer. Part II: Application and evaluation in a mesoscale meteorolog-
1019 ical model. *Journal of Applied Meteorology and Climatology* 46:1396–1409
- 1020 Pohl B, Cr  tat J, Camberlin P (2011) Testing WRF capability in simulating the at-
1021 mospheric water cycle over Equatorial East Africa. *Climate Dynamics* 37:1357–
1022 1379, DOI 10.1007/s00382-011-1024-2
- 1023 Pook MJ, Risbey JS, McIntosh PC (2011) The synoptic climatology of cool-season
1024 rainfall in the Central Wheatbelt of Western Australia. *Monthly Weather Re-*
1025 *view* 140:28–43, DOI 10.1175/MWR-D-11-00048.1
- 1026 Prabha TV, Hoogenboom G, Smirnova TG (2011) Role of land surface param-
1027 eterizations on modeling cold-pooling events and low-level jets. *Atmospheric*
1028 *Research* 99:147 – 161, DOI <http://dx.doi.org/10.1016/j.atmosres.2010.09.017>

- 1029 Raupach MR, Briggs PR, Haverd V, King EA, Paget M, Trudinger CM (2008) Aus-
1030 tralian Water Availability Project. CSIRO Marine and Atmospheric Research,
1031 Canberra, Australia. <http://www.csiro.au/awap>. Accessed 22.10.2009
- 1032 Raupach MR, Briggs PR, Haverd V, King EA, Paget M, Trudinger CM (2009) Aus-
1033 tralian Water Availability Project (AWAP): CSIRO Marine and Atmospheric
1034 Research Component: Final Report for Phase 3. CAWCR Technical Report No.
1035 013. 67 pp.
- 1036 Reason CJC, Gamble D, Pearce AF (1999) The leewind current in the parallel
1037 ocean climate model and applications to regional meteorology and fisheries.
1038 *Meteorological Applications* 6:211–225, DOI 10.1017/S1350482799001255
- 1039 Reynolds RW, Smith TM (1994) Improved global sea surface temperature analyses
1040 using optimum interpolation. *Journal of Climate* 7:929–948
- 1041 Reynolds RW, Rayner NA, Smith TM, Stokes DC, Wang W (2002) An improved
1042 in situ and satellite SST analysis for climate. *Journal of Climate* 15:1609–1625
- 1043 Salathe E, Leung L, Qian Y, Zhang Y (2010) Regional climate model projections
1044 for the state of Washington. *Climatic Change* 102:51–75, 10.1007/s10584-010-
1045 9849-y
- 1046 Schneider DP, Deser C, Fasullo J, Trenberth KE (2013) Climate data guide spurs
1047 discovery and understanding. *Eos, Transactions American Geophysical Union*
1048 94:121–122, DOI 10.1002/2013EO130001
- 1049 Skamarock WC, Klemp JB, Dudhia J, Gill DO, Barker DM, Duda MG, Huang
1050 XY, Wang W, Powers JG (2008) A description of the advanced research WRF
1051 version 3. NCAR Tech. Note NCAR/TN-475+STR, 113 pp., NCAR
- 1052 Smirnova TG, Brown JM, Benjamin SG, Kim D (2000) Parameterization of cold-
1053 season processes in the maps land-surface scheme. *Journal of Geophysical Re-*

- 1054 search: Atmospheres 105(D3):4077–4086, DOI 10.1029/1999JD901047
- 1055 Stéfanon M, Drobinski P, D’Andrea F, Lebeaupin-Brossier C, Bastin S (2013) Soil
1056 moisture-temperature feedbacks at meso-scale during summer heat waves over
1057 western Europe. *Climate Dynamics* pp 1–16, DOI 10.1007/s00382-013-1794-9
- 1058 Tapp RG, Barrell SL (1984) The north-west Australian cloud band: Climatology,
1059 characteristics and factors associated with development. *Journal of Climatology*
1060 4:411–424, DOI 10.1002/joc.3370040406
- 1061 Taylor KE (2001) Summarizing multiple aspects of model performance in
1062 a single diagram. *Journal of Geophysical Research* 106:7183–7192, DOI
1063 10.1029/2000JD900719
- 1064 Yuan X, Liang XZ, Wood E (2012) WRF ensemble downscaling seasonal forecasts
1065 of China winter precipitation during 1982-2008. *Climate Dynamics* 39:2041–
1066 2058, DOI 10.1007/s00382-011-1241-8
- 1067 Zhang Y, Dulière V, Mote PW, Salathé EP (2009) Evaluation of WRF and HadRM
1068 mesoscale climate simulations over the U.S. Pacific Northwest. *Journal of Cli-*
1069 *mate* 22:5511–5526

Table 1: Summary of numerical experiments carried out (BC-boundary conditions, LSM-land surface model, LW-longwave radiation scheme, SW-shortwave radiation scheme, CS-cumulus scheme, PBL-planetary boundary layer scheme, SLS-surface layer scheme, SST-sea surface temperature source, MIC-microphysics scheme)

Experiment	BC	LSM	LW	SW	CS	PBL/SLC	SST	MIC
REF	NNRP	NOAH	RRTM	Dudhia	KF	YSU/MO	NNRP	WSM 5-class
N_SST	NNRP	NOAH	RRTM	Dudhia	KF	YSU/MO	NOAA	WSM 5-class
FNL	FNL	NOAH	RRTM	Dudhia	KF	YSU/MO	NCEP-FNL	WSM 5-class
ERA	ERA-INT	NOAH	RRTM	Dudhia	KF	YSU/MO	ERA-INT	WSM 5-class
RUC	NNRP	RUC	RRTM	Dudhia	KF	YSU/MO	NNRP	WSM 5-class
BMJ	NNRP	NOAH	RRTM	Dudhia	BMJ	YSU/MO	NNRP	WSM 5-class
RTG	NNRP	NOAH	RRTMG	RRTMG	KF	YSU/MO	NNRP	WSM 5-class
CAM	NNRP	NOAH	CAM	CAM	KF	YSU/MO	NNRP	WSM 5-class
AC2	NNRP	NOAH	RRTM	Dudhia	KF	AC2/MO	NNRP	WSM 5-class
AC2_P	NNRP	NOAH	RRTM	Dudhia	KF	AC2/PX	NNRP	WSM 5-class
3C	NNRP	NOAH	RRTM	Dudhia	KF	YSU/MO	NNRP	WSM 3-class
5C_D	NNRP	NOAH	RRTM	Dudhia	KF	YSU/MO	NNRP	WDM 5-class
FNL_RTG	FNL	NOAH	RRTMG	RRTMG	KF	YSU/MO	FNL	WSM 5-class
ERA_RTG	ERA-INT	NOAH	RRTMG	RRTMG	KF	YSU/MO	ERA-INT	WSM 5-class

Table 2: Seasonal absolute and percentage (shown in brackets) bias in maximum temperature ($^{\circ}\text{C}$) for the experiments in Table 1, for the Coastal (Coast), Agricultural (Agric), and Rangelands (Range) regions.

	DJF			MAM			JJA			SON		
	Coast	Agric	Range	Coast	Agric	Range	Coast	Agric	Range	Coast	Agric	Range
REF	-3.3 (-11%)	-3.9 (-12%)	-3.2 (-9%)	-0.7 (-3%)	-1.3 (-5%)	-1.8 (-7%)	-1.9 (-11%)	-1.9 (-6%)	-2.1 (-11%)	-3.0 (-13%)	-2.9 (-12%)	-1.7 (-6%)
N_SST	-3.1 (-11%)	-3.7 (-11%)	-3.1 (-8%)	-0.8 (-3%)	-1.3 (-5%)	-1.5 (-5%)	-1.7 (-10%)	-1.8 (-5%)	-2.1 (-12%)	-3.0 (-13%)	-2.9 (-11%)	-1.6 (-6%)
FNL	-0.7 (-2%)	-1.6 (-5%)	-1.9 (-5%)	0.1 (0%)	-0.4 (-2%)	-0.7 (-3%)	-1.2 (-7%)	-1.6 (-5%)	-1.3 (-7%)	-1.5 (-7%)	-1.7 (-7%)	-1.1 (-4%)
ERA	-0.5 (-2%)	-1.2 (-4%)	-1.5 (-4%)	0.0 (0%)	-0.5 (-2%)	-0.8 (-3%)	-1.3 (-7%)	-1.5 (-5%)	-1.3 (-7%)	-1.5 (-7%)	-1.5 (-6%)	-0.7 (-3%)
RUC	8.9 (31%)	7.9 (24%)	9.8 (27%)	6.0 (26%)	5.6 (22%)	7.1 (26%)	0.6 (4%)	1.9 (6%)	3.5 (19%)	5.8 (26%)	6.9 (27%)	10.5 (40%)
BMJ	-3.2 (-11%)	-3.7 (-11%)	-3.1 (-9%)	-0.6 (-3%)	-1.0 (-4%)	-1.5 (-6%)	-1.8 (-11%)	-1.9 (-6%)	-2.3 (-12%)	-2.5 (-11%)	-2.6 (-10%)	-1.5 (-5%)
RTG	-2.4 (-8%)	-3.0 (-9%)	-2.2 (-6%)	-0.2 (-1%)	-0.4 (-1%)	0.1 (0%)	-0.7 (-4%)	-0.0 (-0%)	0.0 (0%)	-2.1 (-9%)	-1.7 (-7%)	-0.4 (-1%)
CAM	-3.0 (-11%)	-3.7 (-11%)	-2.9 (-8%)	-0.9 (-4%)	-1.3 (-5%)	-1.1 (-4%)	-1.7 (-10%)	-1.4 (-4%)	-1.6 (-9%)	-2.8 (-12%)	-2.5 (-10%)	-1.3 (-5%)
AC2	-3.8 (-13%)	-4.6 (-14%)	-4.0 (-11%)	-0.5 (-2%)	-1.4 (-6%)	-2.2 (-8%)	-1.8 (-11%)	-1.9 (-6%)	-2.1 (-12%)	-3.7 (-16%)	-3.7 (-15%)	-2.5 (-10%)
AC2_P	-1.3 (-5%)	-2.7 (-8%)	-2.0 (-5%)	0.6 (3%)	-0.4 (-1%)	-1.0 (-3%)	-1.9 (-11%)	-1.7 (-5%)	-1.8 (-9%)	-2.7 (-12%)	-2.6 (-10%)	-1.1 (-4%)
3C	-3.2 (-11%)	-3.9 (-12%)	-3.3 (-9%)	-0.9 (-4%)	-1.4 (-5%)	-1.5 (-6%)	-1.7 (-10%)	-1.6 (-5%)	-2.1 (-11%)	-2.9 (-13%)	-2.8 (-11%)	-1.6 (-6%)
5C_D	-3.0 (-10%)	-3.6 (-11%)	-3.0 (-8%)	-0.4 (-2%)	-0.9 (-4%)	-1.5 (-5%)	-1.5 (-9%)	-1.2 (-4%)	-1.4 (-7%)	-2.7 (-12%)	-2.6 (-10%)	-1.5 (-6%)
FNL_RTG	0.3 (1%)	-0.8 (-2%)	-1.5 (-4%)	1.0 (4%)	0.5 (2%)	-0.1 (-0%)	-0.1 (-0%)	-0.0 (-0%)	0.2 (1%)	-0.4 (-2%)	-0.5 (-2%)	-0.1 (-0%)
ERA_RTG	0.1 (0%)	-0.8 (-2%)	-1.4 (-4%)	0.5 (2%)	0.1 (0%)	-0.6 (-2%)	-0.1 (-1%)	0.2 (1%)	0.4 (2%)	-0.5 (-2%)	-0.1 (-1%)	0.3 (1%)

Table 3: Same as in Table 2 except for minimum temperature ($^{\circ}\text{C}$).

	DJF			MAM			JJA			SON		
	Coast	Agric	Range	Coast	Agric	Range	Coast	Agric	Range	Coast	Agric	Range
REF	-2.4 (-17%)	-1.8 (-11%)	-2.9 (-15%)	-1.4 (-12%)	-1.3 (-10%)	-2.9 (-20%)	-1.2 (-19%)	-2.2 (-42%)	-3.0 (-54%)	-1.5 (-16%)	-1.5 (-16%)	-1.9 (-16%)
N_SST	-1.9 (-13%)	-1.2 (-8%)	-2.6 (-13%)	-1.1 (-9%)	-1.3 (-10%)	-3.0 (-21%)	-0.9 (-14%)	-2.2 (-40%)	-3.2 (-58%)	-1.1 (-12%)	-1.3 (-14%)	-1.7 (-15%)
FNL	0.9 (6%)	2.1 (13%)	1.4 (7%)	1.3 (11%)	2.0 (16%)	1.7 (12%)	0.6 (9%)	0.6 (11%)	1.2 (22%)	0.7 (7%)	1.1 (12%)	1.2 (10%)
ERA	0.6 (4%)	1.9 (12%)	1.3 (6%)	1.0 (9%)	1.8 (15%)	1.8 (12%)	0.5 (9%)	0.7 (14%)	1.3 (23%)	0.8 (9%)	1.2 (13%)	1.5 (12%)
RUC	-1.4 (-10%)	-1.1 (-7%)	-1.6 (-8%)	-0.7 (-6%)	-1.2 (-10%)	-2.4 (-17%)	-0.5 (-8%)	-1.4 (-26%)	-2.9 (-52%)	-0.4 (-4%)	0.1 (1%)	-0.5 (-4%)
BMJ	-2.4 (-17%)	-1.6 (-10%)	-2.9 (-14%)	-1.4 (-12%)	-1.4 (-11%)	-3.1 (-22%)	-1.1 (-18%)	-2.5 (-47%)	-3.5 (-63%)	-1.3 (-14%)	-1.4 (-15%)	-1.9 (-16%)
RTG	-1.6 (-11%)	-0.9 (-5%)	-2.0 (-10%)	-0.7 (-6%)	-0.4 (-3%)	-1.3 (-9%)	-0.3 (-5%)	-0.5 (-10%)	-0.9 (-15%)	-0.9 (-10%)	-0.6 (-7%)	-0.6 (-5%)
CAM	-2.8 (-20%)	-2.0 (-12%)	-3.2 (-16%)	-2.1 (-18%)	-2.0 (-16%)	-2.8 (-20%)	-2.2 (-35%)	-2.4 (-45%)	-3.0 (-54%)	-2.1 (-23%)	-1.7 (-18%)	-1.9 (-16%)
AC2	-4.1 (-29%)	-3.5 (-22%)	-5.6 (-28%)	-2.7 (-23%)	-2.9 (-23%)	-5.3 (-38%)	-2.0 (-31%)	-2.8 (-53%)	-3.8 (-69%)	-3.1 (-34%)	-3.3 (-36%)	-4.3 (-36%)
AC2_P	-5.1 (-36%)	-4.5 (-28%)	-6.4 (-32%)	-3.5 (-30%)	-3.7 (-30%)	-6.4 (-45%)	-3.0 (-47%)	-4.0 (-75%)	-5.4 (-97%)	-4.0 (-43%)	-4.2 (-45%)	-5.6 (-48%)
3C	-2.4 (-16%)	-1.7 (-11%)	-3.1 (-15%)	-1.6 (-14%)	-1.6 (-13%)	-2.9 (-21%)	-1.3 (-20%)	-2.2 (-41%)	-3.1 (-56%)	-1.5 (-16%)	-1.6 (-17%)	-1.9 (-16%)
5C.D	-2.3 (-16%)	-1.7 (-11%)	-2.8 (-14%)	-1.1 (-9%)	-0.9 (-8%)	-2.6 (-19%)	-0.8 (-12%)	-1.7 (-32%)	-2.4 (-43%)	-1.4 (-15%)	-1.3 (-14%)	-1.7 (-15%)
FNL_RTG	1.3 (9%)	2.6 (16%)	1.9 (9%)	1.8 (16%)	2.8 (23%)	2.6 (19%)	1.4 (23%)	1.9 (35%)	2.8 (50%)	1.4 (15%)	2.1 (23%)	2.4 (20%)
ERA_RTG	1.1 (7%)	2.5 (15%)	1.8 (9%)	1.6 (14%)	2.6 (21%)	2.5 (18%)	1.4 (22%)	1.9 (36%)	2.9 (52%)	1.5 (16%)	2.2 (24%)	2.5 (21%)

Table 4: Same as in Table 2 except for precipitation (mm month^{-1}).

	DJF			MAM			JJA			SON		
	Coast	Agric	Range	Coast	Agric	Range	Coast	Agric	Range	Coast	Agric	Range
REF	4.1 (117%)	-0.1 (-1%)	-8.4 (-87%)	-18.9 (-38%)	-20.0 (-68%)	-18.3 (-82%)	-13.3 (-14%)	-21.4 (-55%)	-15.4 (-83%)	-6.9 (-20%)	-4.1 (-34%)	-13.2 (-91%)
N_SST	5.3 (150%)	1.1 (20%)	-8.4 (-87%)	-16.5 (-33%)	-19.8 (-67%)	-19.7 (-89%)	-3.8 (-4%)	-18.1 (-46%)	-15.5 (-83%)	-2.0 (-6%)	-3.2 (-26%)	-13.0 (-89%)
FNL	7.2 (206%)	7.3 (141%)	9.5 (99%)	-16.1 (-32%)	-7.9 (-27%)	5.8 (26%)	12.6 (14%)	3.5 (9%)	6.0 (32%)	-0.9 (-2%)	3.2 (27%)	-4.2 (-29%)
ERA	2.2 (62%)	2.6 (49%)	8.9 (92%)	-9.9 (-20%)	-4.1 (-14%)	9.6 (44%)	6.8 (7%)	-0.7 (-2%)	4.1 (22%)	3.8 (11%)	2.3 (19%)	-4.3 (-30%)
RUC	4.6 (132%)	-0.3 (-7%)	-8.3 (-86%)	-22.7 (-45%)	-21.7 (-74%)	-19.6 (-89%)	-19.1 (-20%)	-20.1 (-51%)	-13.9 (-74%)	-9.4 (-27%)	-5.0 (-41%)	-13.1 (-91%)
BMJ	2.7 (75%)	-1.8 (-34%)	-8.8 (-91%)	-26.9 (-54%)	-23.9 (-81%)	-20.4 (-92%)	-24.4 (-26%)	-21.2 (-54%)	-15.1 (-81%)	-14.4 (-42%)	-6.2 (-51%)	-13.7 (-95%)
RTG	4.1 (116%)	-0.3 (-5%)	-8.6 (-89%)	-21.4 (-43%)	-19.0 (-64%)	-19.5 (-88%)	-21.0 (-23%)	-20.5 (-52%)	-15.5 (-83%)	-12.2 (-35%)	-6.3 (-52%)	-13.3 (-92%)
CAM	3.2 (90%)	-0.1 (-2%)	-8.5 (-88%)	-19.4 (-39%)	-20.0 (-68%)	-17.7 (-80%)	-17.4 (-19%)	-19.7 (-50%)	-15.2 (-82%)	-12.5 (-36%)	-5.2 (-43%)	-12.9 (-89%)
AC2	4.6 (131%)	-0.4 (-8%)	-7.8 (-80%)	-20.9 (-42%)	-21.9 (-74%)	-19.4 (-88%)	-6.2 (-7%)	-17.4 (-44%)	-14.9 (-80%)	-6.1 (-18%)	-3.1 (-25%)	-12.6 (-87%)
AC2_P	3.4 (98%)	-0.4 (-7%)	-8.5 (-88%)	-16.1 (-32%)	-21.5 (-73%)	-19.5 (-88%)	-3.2 (-3%)	-14.5 (-37%)	-14.3 (-76%)	-4.1 (-12%)	-2.5 (-21%)	-12.9 (-89%)
3C	3.7 (105%)	0.5 (10%)	-8.3 (-86%)	-20.0 (-40%)	-21.4 (-72%)	-19.0 (-86%)	-17.0 (-18%)	-21.7 (-55%)	-15.6 (-84%)	-7.8 (-23%)	-4.7 (-39%)	-13.2 (-91%)
5C_D	5.7 (163%)	0.2 (3%)	-8.2 (-84%)	-15.0 (-30%)	-17.8 (-60%)	-18.9 (-86%)	-8.9 (-10%)	-19.1 (-49%)	-14.8 (-79%)	-5.5 (-16%)	-3.1 (-25%)	-13.0 (-89%)
FNL_RTG	5.6 (160%)	7.6 (146%)	22.3 (230%)	-19.3 (-39%)	-3.5 (-12%)	19.0 (86%)	4.2 (5%)	8.3 (21%)	10.0 (53%)	-2.9 (-8%)	4.6 (38%)	1.2 (8%)
ERA_RTG	3.7 (106%)	7.5 (145%)	21.3 (220%)	-10.8 (-22%)	3.5 (12%)	25.3 (114%)	-0.9 (-1%)	-2.6 (-7%)	3.6 (19%)	-4.5 (-13%)	2.4 (20%)	2.9 (20%)

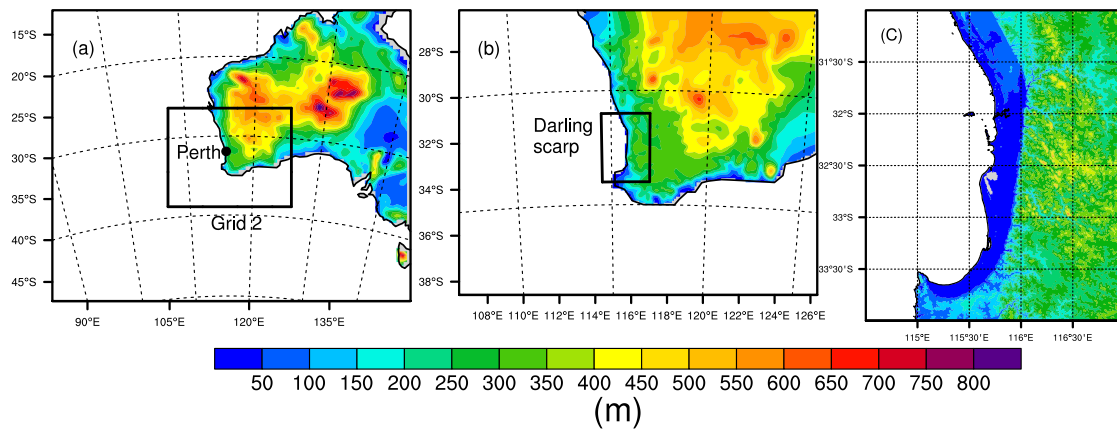


Fig. 1: (a) Map showing the topography of the outer grid domain (50-km resolution), the boundary of the second inner nested grid representing SWWA, and the location of the city of Perth; (b) topography of the second inner nested domain (10-km resolution) and location of the Darling scarp, and; (c), topography of the Darling scarp (9-arc seconds topography from Geoscience Australia (Hutchinson et al, 2009)). Note that the maps shown in (a) and (b) are the computational grids used for the simulations whereas the map shown in (c) is only for the purpose of illustrating the sharp increase in topography associated with the Darling scarp.

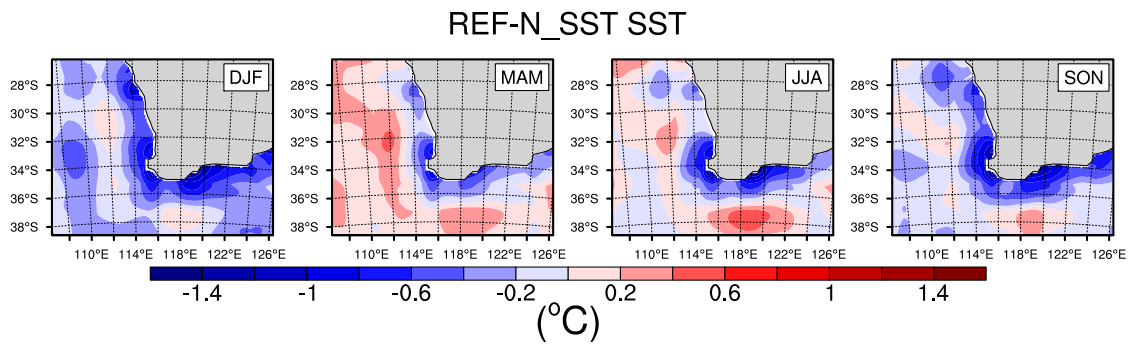


Fig. 2: Countour plots showing the difference in sea surface temperature between the REF and N_SST experiments (C) by season. Negative values indicate that the N_SST simulation had higher sea surface temperatures relative to REF.

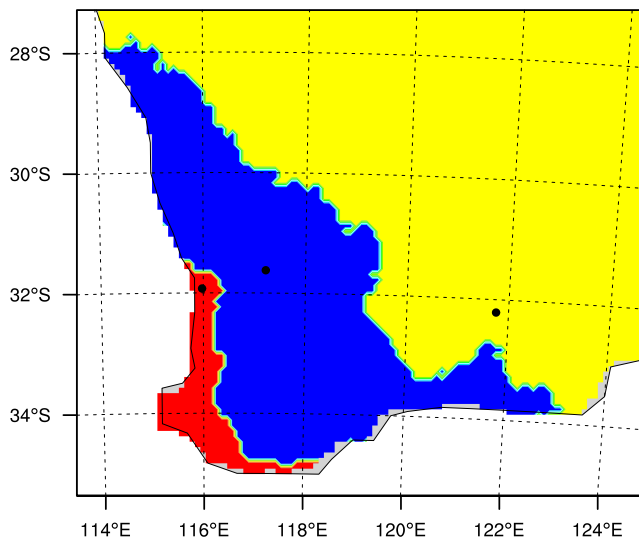


Fig. 3: Regionalisation used during analysis (red = coast, blue = agricultural region, yellow = rangelands). Each black dot in the 3 regions represent the location of a precipitation station used for further analysis, namely, the Perth Airport station at the coast, the Cunderdin in the agricultural region, and Norseman in the rangelands.

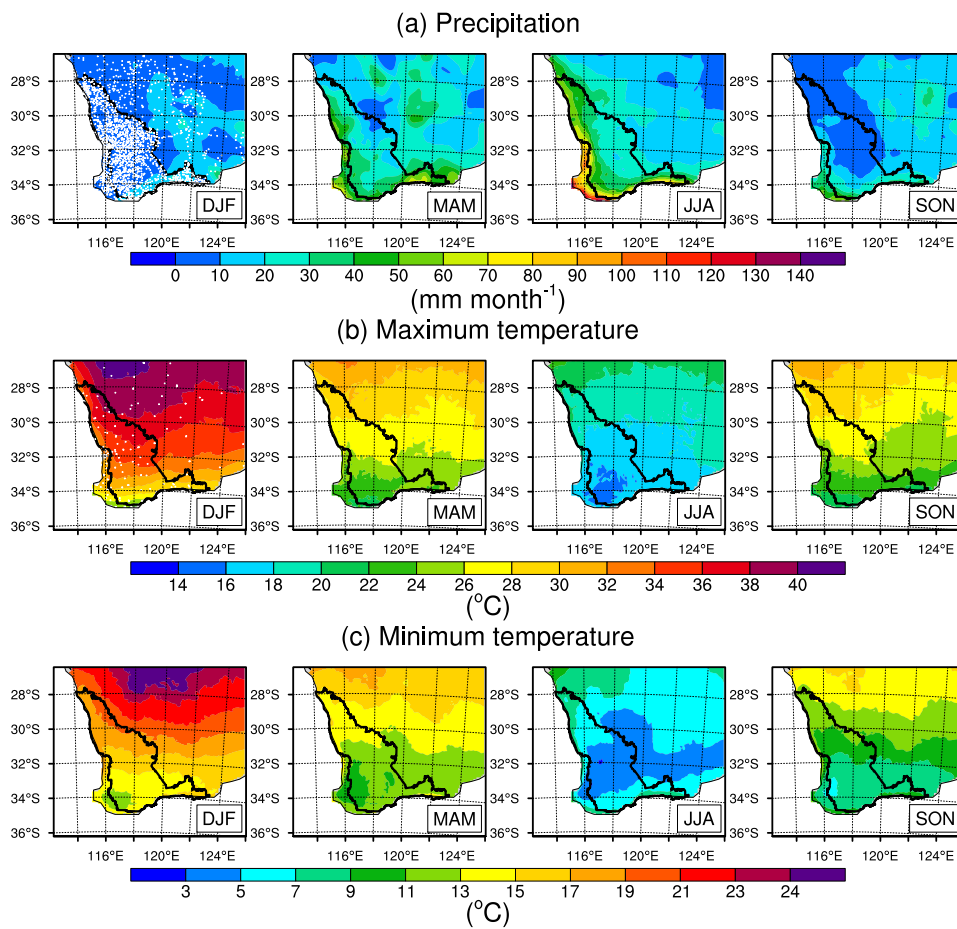


Fig. 4: (a) Precipitation (mm month^{-1}), (b) maximum temperature ($^{\circ}\text{C}$), and (c) minimum temperature over SWWA during DJF, MAM, JJA, and SON of 2010 from the Australian Bureau of Meteorology. White dots in the DJF panels (a) and (b) show precipitation and temperature station locations and the black solid line represents the approximate boundaries of the agricultural region.

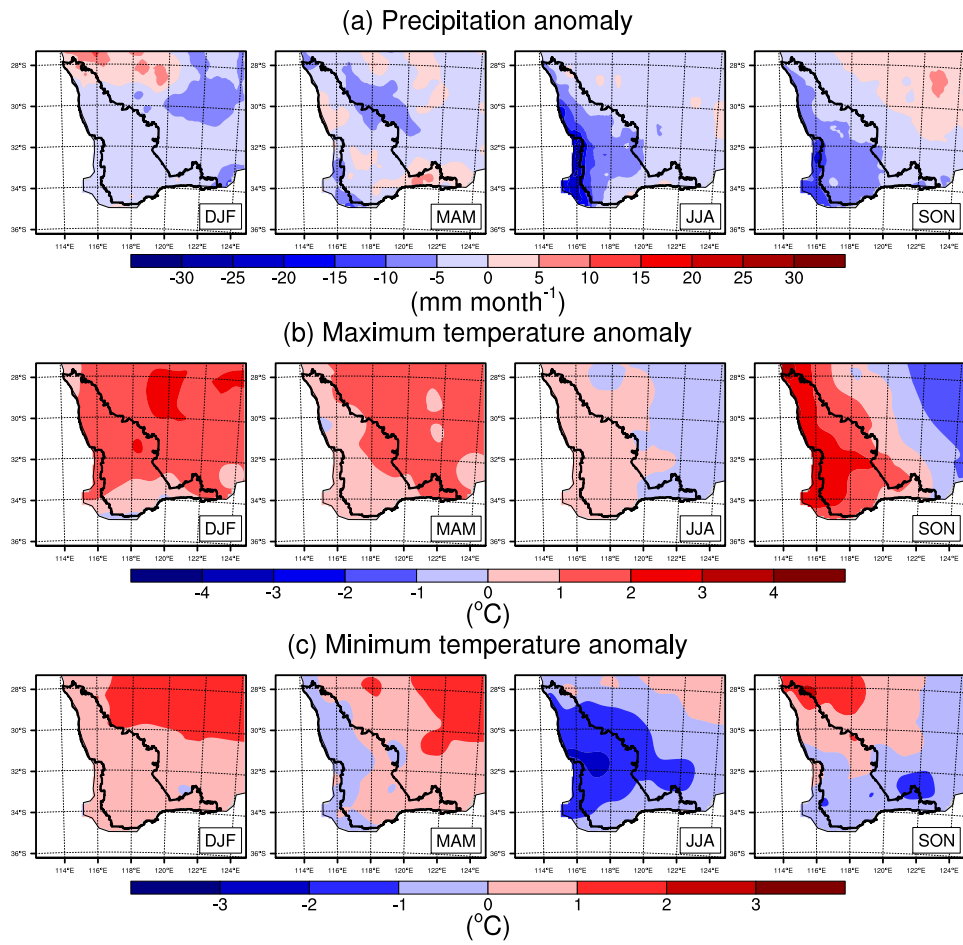


Fig. 5: Same as in Fig. 4 except showing the seasonal 2010 anomaly from 1970-2010.

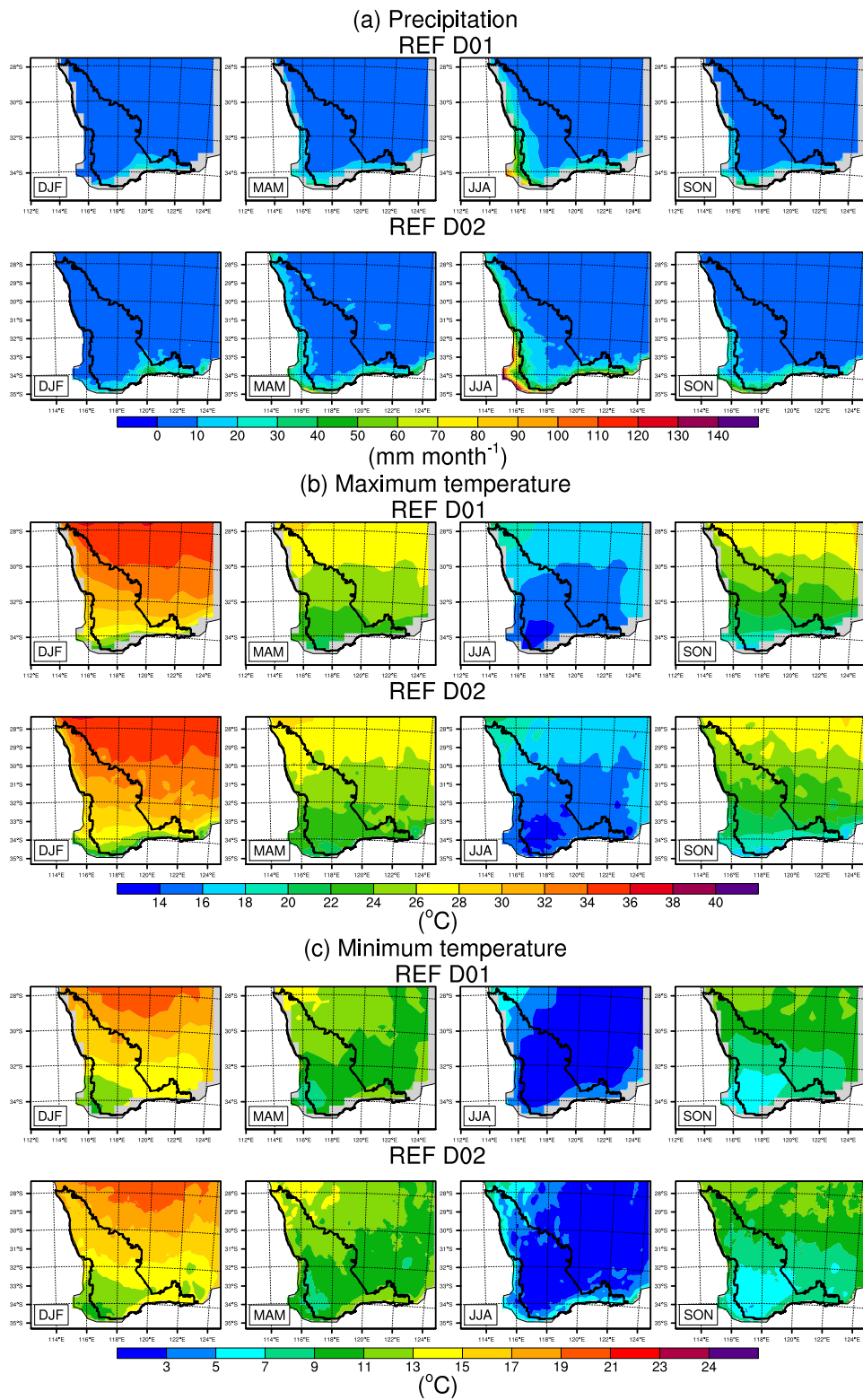


Fig. 6: (a) Precipitation (mm month^{-1}), (b) maximum temperature ($^{\circ}\text{C}$), and (c) minimum temperature over SWWA during DJF, MAM, JJA, and SON of 2010 from the outer 50-km domain (D01) and inner 10-km nested domain (D02) for the REF experiment (Table 1).

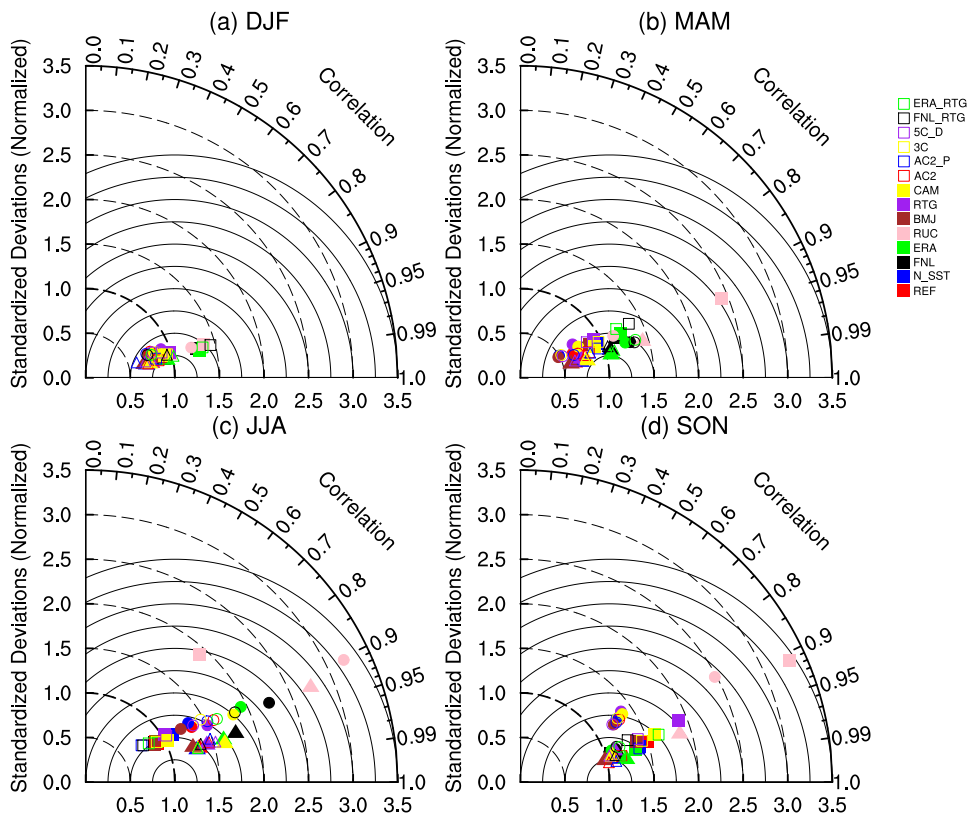


Fig. 7: Taylor diagrams for maximum temperature during (a) DJF, (b) MAM, (c) JJA, and (d) SON, for the experiments in Table 1, for the coastal region (squares), the agricultural region (triangles), and rangelands (circles).

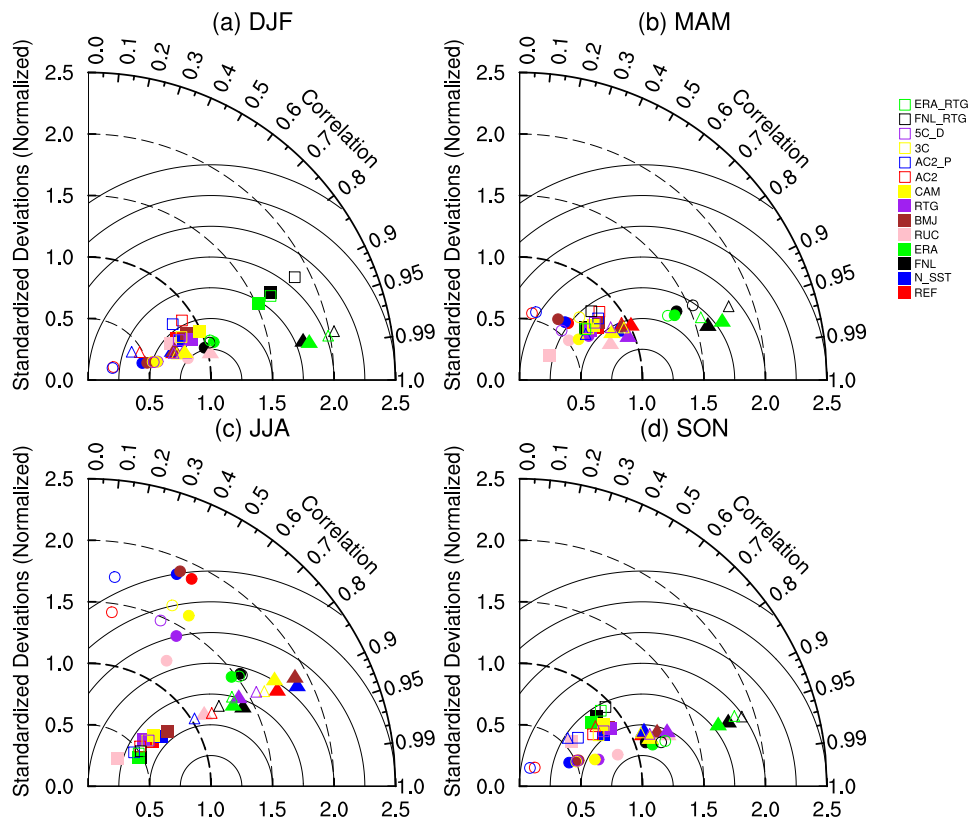


Fig. 8: Same as in Figure 7, except for minimum temperature.

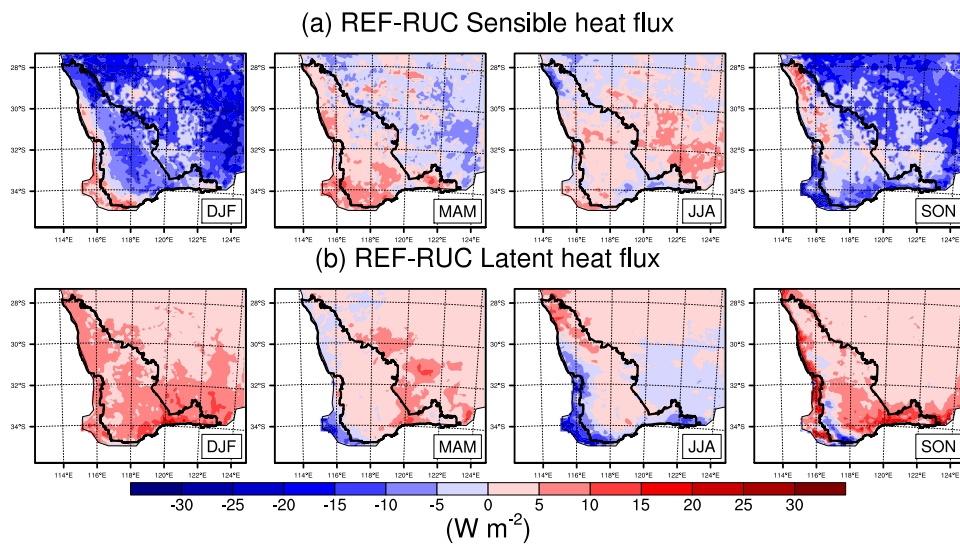


Fig. 9: Differences in seasonal (a) sensible, and (b) latent heat flux (W m^{-2}) between the REF and RUC experiments (Table 1)

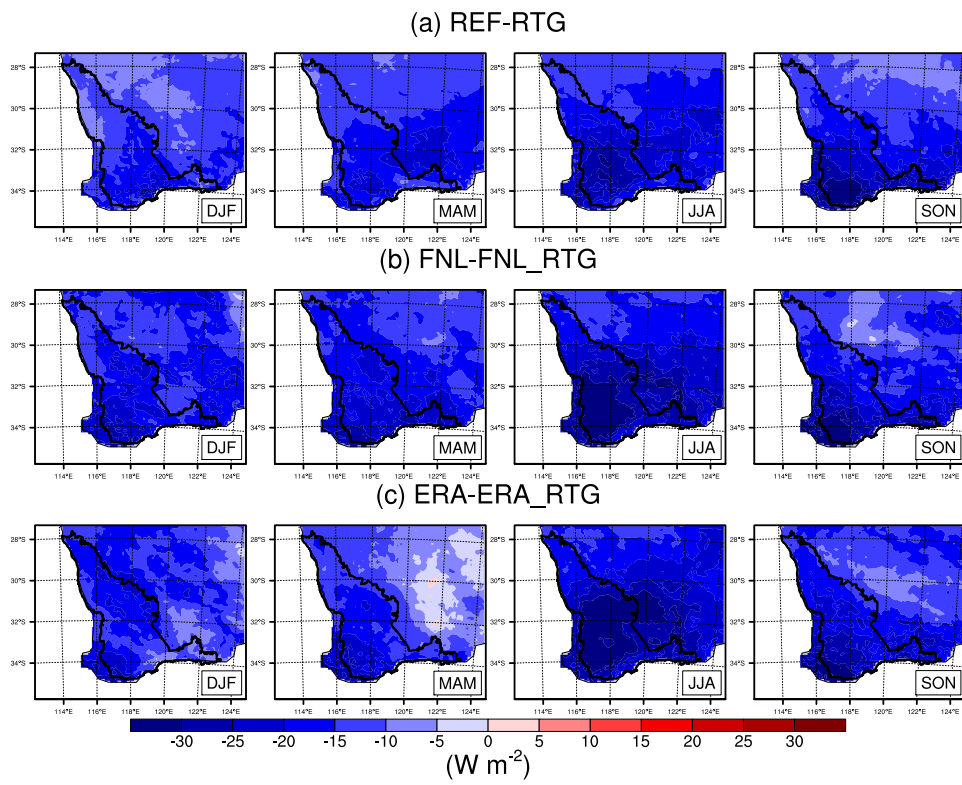


Fig. 10: Seasonal means of differences in incoming shortwave radiation (W m^{-2}) between the (a) REF and RTG, (b) FNL and FNL_RTG, and (c) ERA and ERA_RTG experiments (Table 1).

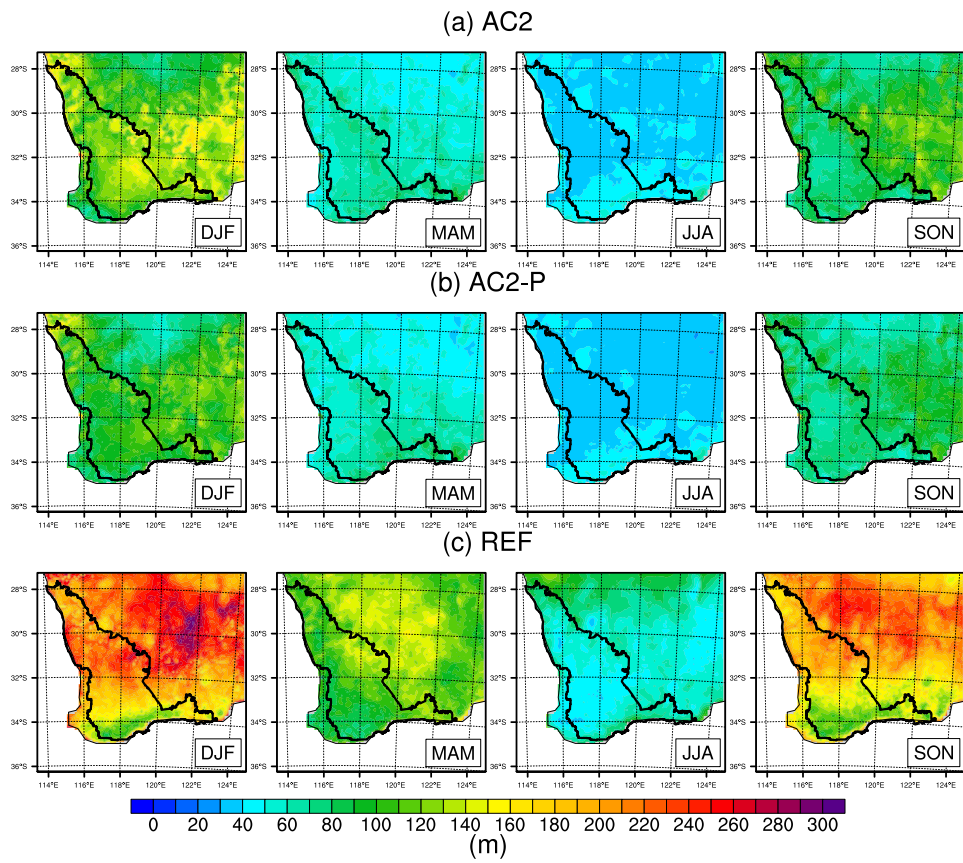


Fig. 11: Seasonal means of minimum PBL heights for (a) AC, (b) AC2_P, and (c) REF simulations (Table 1).

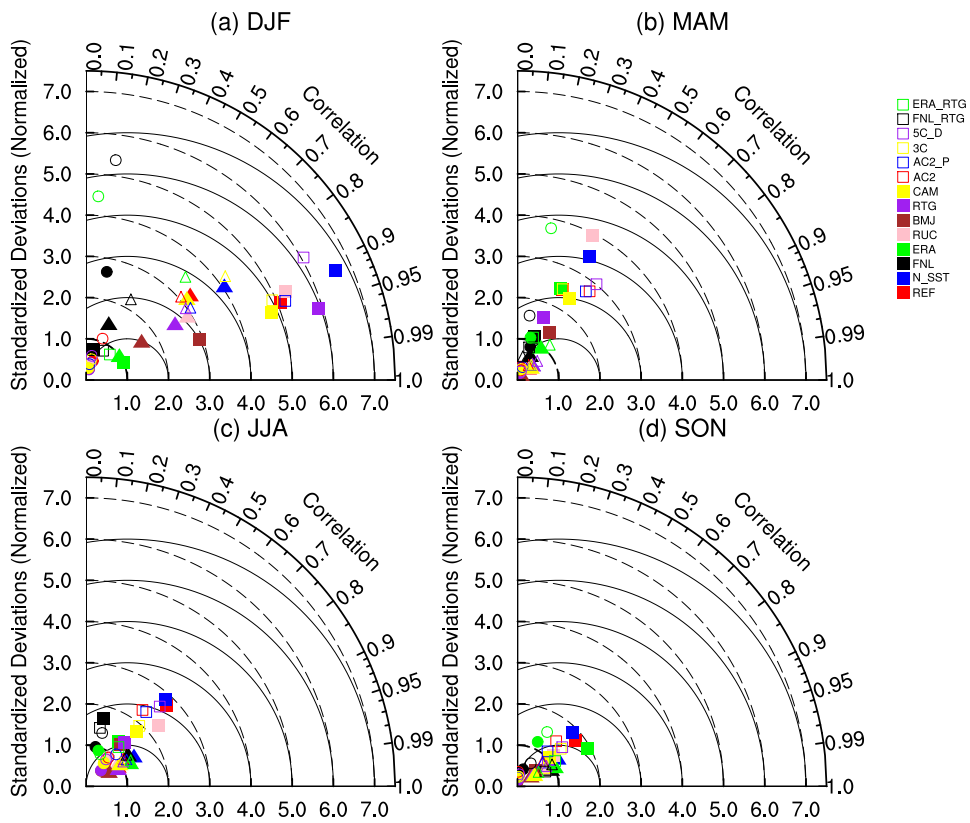


Fig. 12: Same as in Figure 7, except for precipitation.

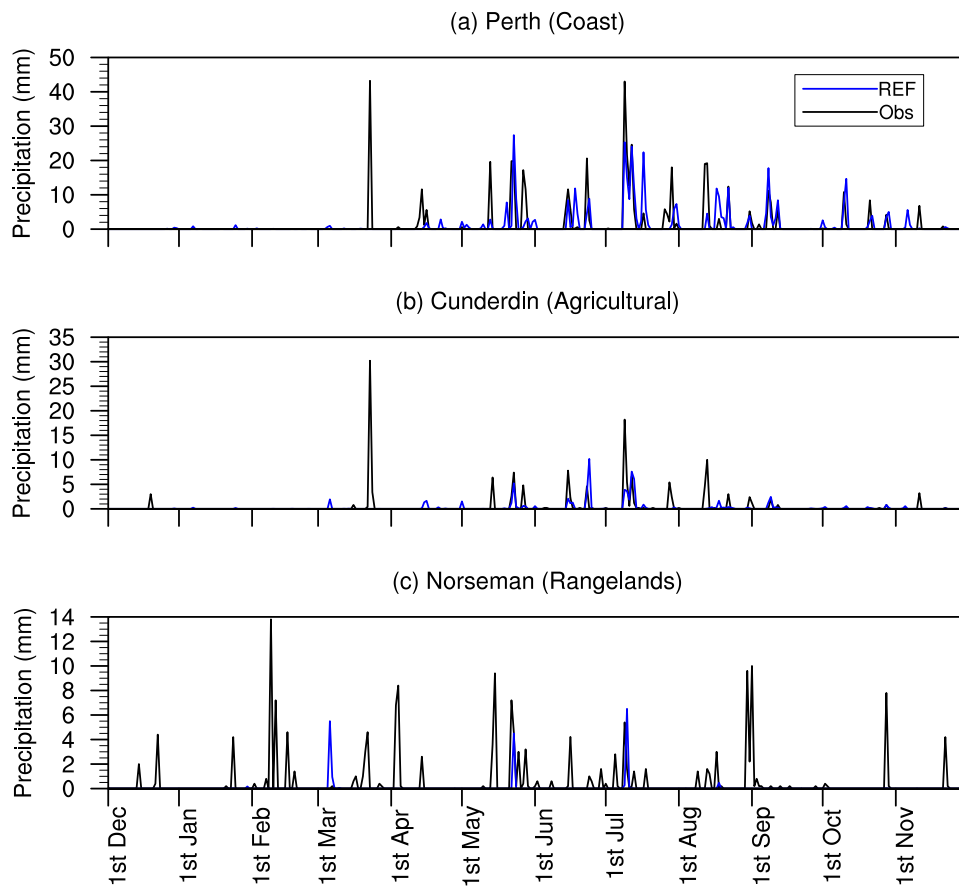


Fig. 13: Time series of daily precipitation (mm) from 1st of December 2009 to 30th of November 2010 at the: (a) Perth (Coast), (b) Cunderdin (Agricultural), and (c) Norseman (Rangelands) stations (Fig. 3). Black lines represent the observations and the blue lines the REF experiment.

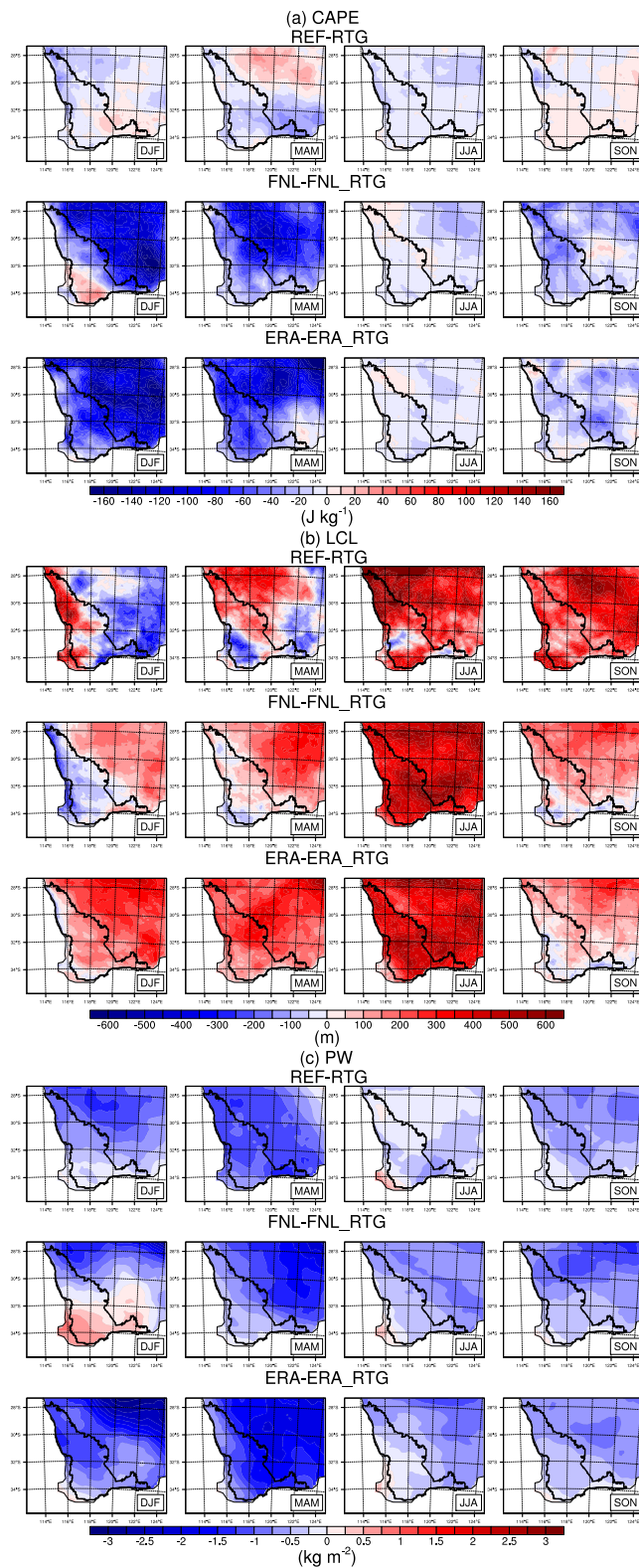


Fig. 14 Differences in: (a) Convective Available Potential Energy (CAPE) (J kg^{-1}), (b) Lifting Condensation Level (LCL) (m), and (c) Precipitable Water (PW) (kg m^{-2}) between the REF and RTG (REF-RTG), FNL and FNL_RTG (FNL - FNL_RTG), and ERA and ERA_RTG (ERA - ERA_RTG) experiments (Table 1).